LIQUIDUS SURFACE FOR THE HIGH CRYOLITE/LOW ALUMINA PORTION OF THE Na_3AlF_6-AlF_3-CaF_2-Al_2O_3 SYSTEM

by

Ming-Wei Paul Xu

Thesis submitted to the Graduate Faculty of the
Virginia Polytechnic Institute and State University
in partial fulfillment of the requirements
for the degree of

MASTER OF SCIENCE

in

Materials Engineering

APPROVED:

J. J. Brown, Jr., Chairman

G. V. Gibbs

J. L. Lytton

May, 1983

Blacksburg, Virginia

LIQUIDUS SURFACE FOR THE HIGH CRYOLITE/LOW ALUMINA PORTION OF THE Na_3AlF_6-AlF_3-CaF_2-Al_2O_3 SYSTEM

by

Ming-Wei Paul Xu

(ABSTRACT)

The purpose of this work was to determine the liquidus surface of the cryolite-rich portion of the ternary system Na_3AlF_6-CaF_2-AlF_3 and to establish the effect of Al_2O_3 on the operation of the Hall cell electrolysis. A series of isotherm of the cryolite-rich portion were graphed.

It was shown that pseudo-binary phase diagrams of Al_2O_3 and bulk composition in the cryolite-rich portion of the Na_3AlF_6-CaF_2-AlF_3 system were found to be simple eutectic. The temperatures and the alumina contents of the double solubility limit, two important parameters for the Hall cell, of the joins 95 Na_3AlF_6/5 AlF_3-$NaCaAlF_6$, 90 Na_3AlF_6/ 10 $NaCaAlF_6$ and 85 Na_3AlF_3/15 AlF_3-$NaCaAlF_6$ were determined.

The cryolite liquidus temperature of the quaternary system Na_3AlF_6-CaF_2-AlF_3-Al_2O_3 was found to be expressed by:

$$T_{Liq.}(\,C) = 1009.4 + 4.059(CaF_2) - 1.167(CaF_2)^2 + 0.968 \times (CaF_2)(AlF_3) - 0.105(CaF_2)(AlF_3)^2 + 0.073 \times (CaF_2)^2(AlF_3) + 0.002(CaF_2)^2(AlF_3)^2 - 4.165 \times (AlF_3) - 0.054(AlF_3)^2 - 5.33(Al_2O_3)$$

for CaF_2 3.8∿11.25%, AlF_3 5∿20%.

ACKNOWLEDGEMENTS

The author wishes to express his appreciation from the bottom of his heart to the Chairman of his Graduate Committee Dr. J. J. Brown, Jr., for his support and invaluable guidance throughout the course of this work. He also appreciates Dr. C. W. Spencer, Head of Department of Materials Engineering, Virginia Polytechnic Institute and State University for his support and concern.

The author sincerely thanks Dr. R. Morena for his enthusiastic guidance, help and encouragement in every aspect of this work within the past fifteen months.

The author also wishes to express thanks to Dr. G. V. Gibbs and Dr. J. L. Lytton for their careful correction of his thesis, giving valuable advice and serving on his graduate committee.

The author would like to thank Dr. John White, Division of Mineralogy, U.S. National Museum for offering the sample of chiolite.

This work was sponsored by a contract from the Aluminum Company of America (ALCOA).

TABLE OF CONTENTS

TABLE OF CONTENTS (CONT'D)

LIST OF FIGURES

LIST OF FIGURES (CONT'D)

LIST OF TABLES

I. INTRODUCTION

A. Background

Today, aluminum is a widely used and important metal; however, as recent as the last century, aluminum was as expensive as gold [1]. This high cost for aluminum was due to the strong affinity of aluminum and oxygen, consequently it is very difficult to produce aluminum by reduction of Al_2O_3 obtained from bauxite by the Bayer process. Theoretically, aluminum can be produced by electrolyzing molten Al_2O_3. However, Al_2O_3 is an extremely refractory material; its melting point is so high (2054°C) that it is impractical to electrolyze molten Al_2O_3 on a commercial scale.

In 1886, Hall and Heroult found a good electrolyte, i.e., molten cryolite solution, in which alumina could be readily dissolved. The liquidus temperature of this solution was less than 1000°C (usually ~950°C), much lower than that of alumina. As a result of this process, aluminum could be produced inexpensively on a large scale.

The container used to electrolyze Al_2O_3 is called the Hall cell (Fig. 1). The total reaction that occurs is:

$$\frac{1}{2}\,Al_2O_3 + \frac{3}{4}C_{(anode)} = Al_{(l)} + \frac{3}{4}\,CO_2 \qquad (1)$$

and the product (molten aluminum) settles to the bottom of the cell.

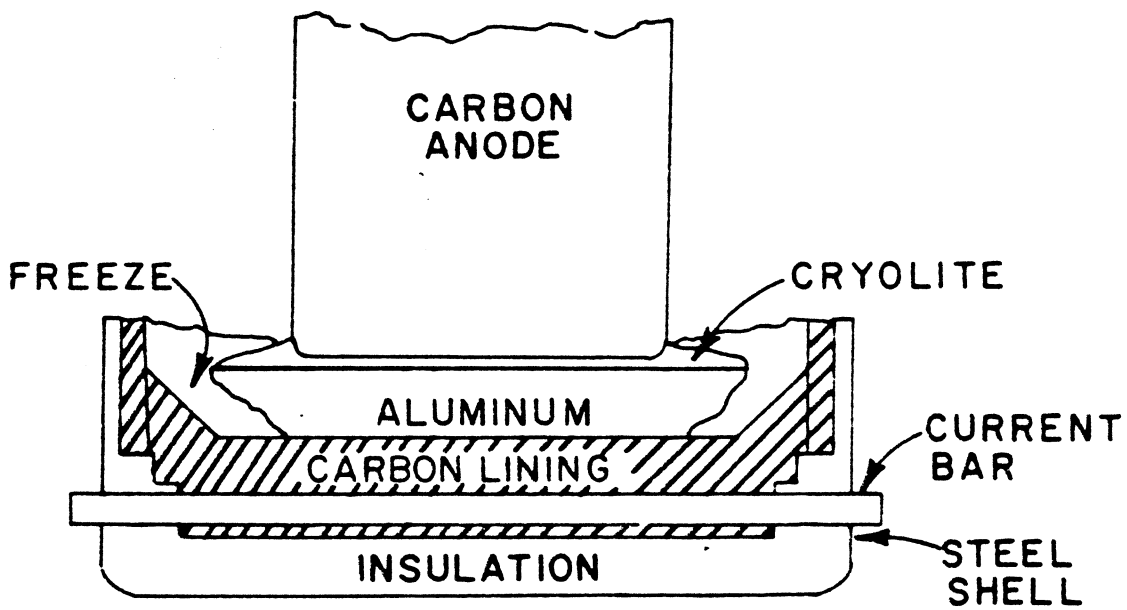

Fig. 1. Reduction cell (schematic).
Operating voltage 4-6 v.
Anode current density 0.7 A/cm^2.

From a technical and economic point of view, the process is not perfect; for example, the energy consumption is high, usually 6-8 KwH/Lb. Al [2]. Therefore, the need to decrease the energy consumption in the Hall process is a primary concern of the aluminum industry.

There are two main causes for the excessive energy consumption in the production of aluminum:

1) Inverse reaction - During electrolysis, some molten aluminum reacts with CO_2 dissolved in the cryolite solution according to the reaction:

$$Al_{(1)} + \frac{3}{2} CO_2 \longrightarrow \frac{1}{2} Al_2O_3 + \frac{1}{2} CO \qquad (2)$$

A fraction of the aluminum formed is reoxidized, so that the net gain of aluminum is less than the amount calculated by Faraday's law. The current efficiency (CE) of the Hall cell is defined as:

$$CE = \frac{\text{The actual amount of aluminum deposited on the cathode}}{\text{The theoretical amount of aluminum deposited on the cathode according to Faraday's law.}} \qquad (3)$$

Usually, CE = 85∿92%. If CE is improved by 5% (e.g. from 90% to 95%) energy consumption can be reduced by 0.4 KwH/Lb. Al. In 1980, Alcoa reported a test campaign with a CE of 94.6% [3].

In order to improve CE, it is recommended that the following be adopted.

a) Lowering the operation temperature - If the operating temperature is lowered, both the aluminum solubility in the cryolite solution and the diffusivity are lowered so that the rate of the inverse reaction decreases. Consequently, the current efficiency increases if we suppose the primary reaction (1) is unchanged with temperature. It has been shown that when the bath temperature is lowered by 10°C, the current efficiency will be increased by 1% and the production cost will be lowered by $7.40/Ton Al [4].

The addition of Al_2O_3 and various fluorides (e.g. AlF_3, CaF_2, LiF, etc.) can lower the melting point of the cryolite solution, and thus decrease the operating temperature and improve current efficiency. However, important physicochemical properties of the bath (e.g. viscosity, density, interfacial tension, etc.) are also affected by these additives. Therefore, there is an optimum operating temperature for any given bath composition.

b) Adjusting the density of the cryolite solution - In order to decrease the inverse reaction. the density of the cryolite solution should be less than that of molten aluminum (2.3 g/c.c.). Usually, it is adjusted at 2.1 g/c.c. by adding AlF_3, LiF, CaF_2, etc.

c) Adjusting the viscosity of the electrolyte - Because the rate of the inverse reaction depends on mass

transfer of reactants and products in the electrolyte, which in turn depends on the viscosity of the electrolyte, the viscosity is also an important property. Viscosity is controlled by adjusting the CaF_2 content.

d) Increasing interfacial tension - Because of the high interfacial tension (∿460 MN/m) between the cryolite solution and molten aluminum, the alumina particles which are added periodically settle at the aluminum/bath interface, rather than at the bottom of the cell. The alumina particles remain there until they are dissolved [5]. These alumina particles inhibit dissolution of molten aluminum into the cryolite solution, and, consequently lower the rate of the inverse reaction.

In general, the more Al_2O_3 added into the electrolyte, the higher the interfacial tension, and the higher the current efficiency [5].

2) The high voltage of the cell - Bratland et al [6] indicated that the theoretical voltage (i.e. the reversible voltage) of the cell was 1.17 v. at CE = 90%. However, the operating voltage of a typical cell is 4-6 v. The large difference between these values is due to over-voltage, voltage drop in the bath because of the Ohmic resistance of the electrolyte, voltage drop in anode and cathode parts, etc.

As a result of the inverse reaction and over-voltage, only part of the energy is available for electrolyzing Al_2O_3. This available energy is generally expressed as the energy efficiency (EE), which is defined as the ratio of energy required to energy input for producing 1 lb. aluminum.

$$EE = \frac{\text{Energy required for producing 1 lb. aluminum}}{\text{Energy input to produce 1 lb. aluminum}} \quad (4)$$

According to a calculation by Bratland [6].

$$EE = \frac{0.481 + 1.65\ (CE)}{V_{cell}} \quad (5)$$

If CE = 85 ~ 92%, V = 4-6 v., then EE ≈ 40%.

It is vital to every aluminum manufacturer to attempt to improve the energy efficiency of the Hall cell. This can be accomplished by increasing CE and/or decreasing V_{cell} by altering the composition of the bath, changing the operating temperature, decreasing the over-voltage, decreasing the voltage drop by using TiB_2 as a stable cathode [2], using graphite cathode blocks in a quasi monolithic construction [7] and employing non-consumable anodes [8].

Nevertheless, the effect of bath composition on energy efficiency is so great that tremendous work has been done in seeking a better composition range, optimum operating temperature, density, viscosity, interfacial tension and the electrical conductivity of the electrolyte. No additive can simultaneously fulfill all the requirements mentioned above;

therefore, the function of each additive must be considered.

1) Al_2O_3. Since aluminum is produced by electrolyzing alumina dissolved in the cryolite solution, it is the fundamental component in the electrolyte.

In a commercial Hall cell, the higher the alumina content, the higher the interfacial tension between the cryolite solution and molten aluminum and the higher the current efficiency. For example, if the alumina content increases from 2 wt.% to 4 wt.% to 6 wt.%, CE increases from 84% to 90% to 92% [4]. Furthermore, if the alumina content is lowered below 2 wt.%, the voltage of the cell will abruptly increase 30 $\sim$ 50% and energy efficiency will decrease dramatically. This phenomenon is called the "anode effect". This is why alumina should be added periodically to keep its content in the electrolyte at a high level (at least 3$\sim$5 wt.%).

However, there are some limitations. Alumina increases the electrical resistance [9] and the density of the cryolite solution, both of which lower the energy efficiency. Furthermore, from Fig. 2 and Fig. 3 which show the Na_3AlF_6-Al_2O_3 binary phase diagram and the CaF_2, AlF_3-containing cryolite solution - Al_2O_3 pseudo binary liquidus diagram, it can be seen that the liquidus line in the hypereutectic region is much steeper than in the hypoeutectic portion. This means the addition or consumption of Al_2O_3 during operation will seriously affect the stability of operation if the composi-

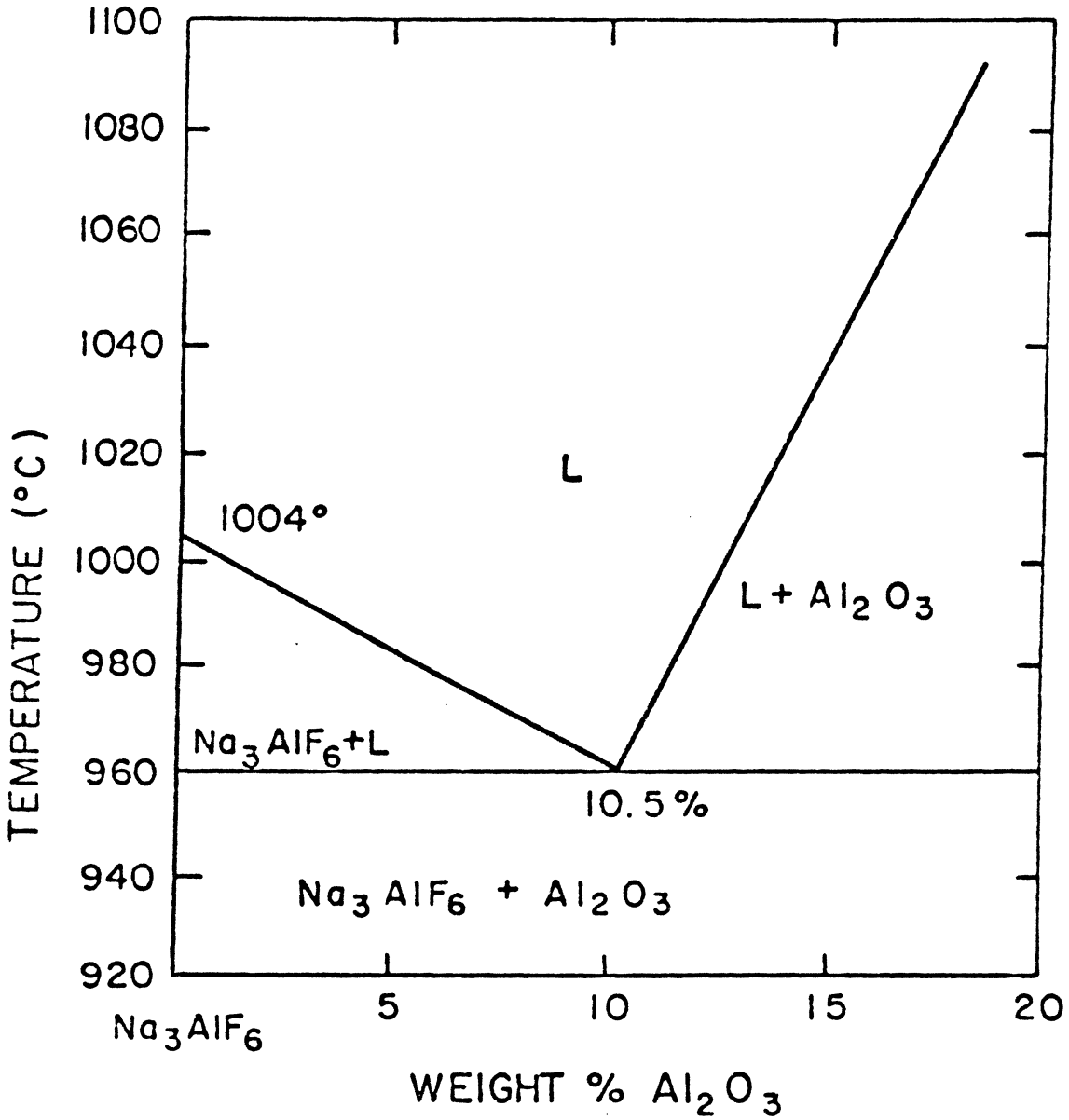

Fig. 2. System Na_3AlF_6-Al_2O_3.[10]

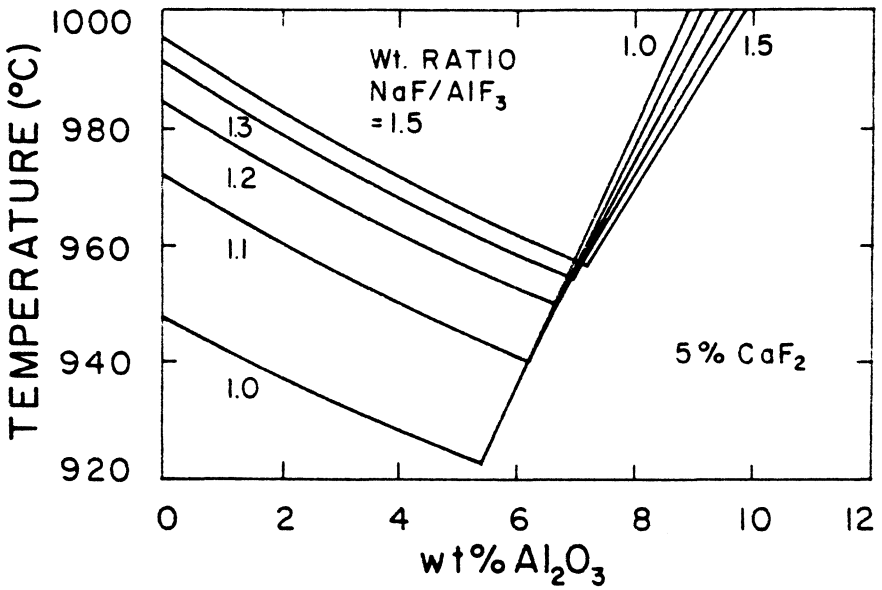

(a)

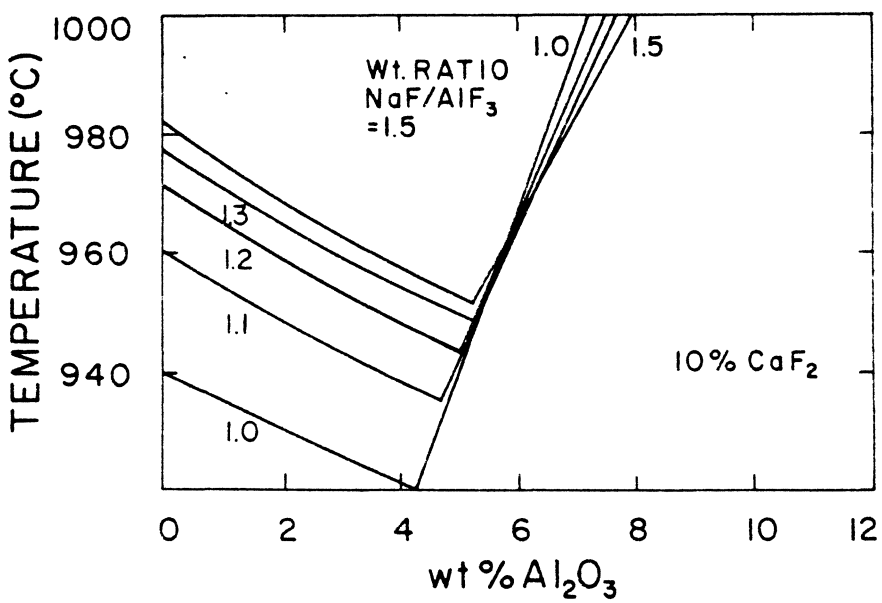

(b)

Fig. 3. Pseudo-binary liquidus diagram[11] (obtained from the calculation of Dewing's expression).

tion of the electrolyte is hypereutectic and the Al_2O_3 content is too high. Consequently, it is recommended that the alumina content of the electrolyte be hypoeutectic and near the eutectic (usually, the eutectic alumina content is $< 5 \sim 6$ wt.%) so that the melting point will be lowest. The operating temperature of the Hall cell is generally 20°C above the eutectic temperature.

2) AlF_3. During heating, cryolite will decompose to NaF and AlF_3 according to the reaction

$$Na_3AlF_6 \longrightarrow 3NaF + AlF_3 \qquad (6)$$

for pure cryolite, the cryolite ratio (CR) $\frac{NaF}{AlF_3}$ equals 3:1 (atomic percent basis)* or 1.5 if weight percent is used.

From Fig. 3, it is obvious that no matter how large the CaF_2 content is, the lower the cryolite ratio, the lower the eutectic temperature. Therefore, in order to lower the operating temperature, some excess AlF_3 must be added to the cryolite solution. Meanwhile, the addition of AlF_3 can decrease the density of the electrolyte and increase the interfacial tension between the cryolite solution and molten aluminum [12]. This in turn will decrease the rate of the inverse reaction.

---

*Some work showed that this ratio was 2.824 [11].

However, the cryolite ratio cannot be too low. First, when the cryolite ratio is decreased to 1.1 ∿ 1.0, the eutectic Al_2O_3 content is so low that the requirement of eutectic alumina content equal to 5-6 wt.% cannot be fulfilled; thus the current efficiency will be lower; second, the addition of AlF_3 into the electrolyte increases electrical resistance of the electrolyte. As a result, energy efficiency will decrease.

For these reasons, the cryolite ratio is usually controlled at ∿1.25. This means that 5-10 wt.% AlF_3 is added to the cryolite solution.

3) CaF_2. CaF_2 lowers the cryolite liquidus temperature (cf. Fig. 3a and 3b), but its effect on the eutectic temperature is not great, being only 1°C/1 wt.% CaF_2 [11]. The main function of CaF_2 is to adjust the viscosity and density of the electrolyte.

However, because of its influence in lowering the eutectic alumina content and increasing the electrical resistance of the electrolyte, the desirable content of CaF_2 is 4-6 wt.%, which corresponds to CR 1.2 ∿ 1.35 (i.e. 5-10% AlF_3) and an electrolyte density of 2.095 ∿ 2.115 g/c.c.

4) LiF and MgF_2. The functionsof LiF and MgF_2 are to decrease the electrical resistance [13] as well as to lower the melting point of the electrolyte.

Nevertheless, any Li and Mg present in the final product will degrade aluminum, so that LiF and MgF_2 in the cryolite

solution are restricted to 0.1 wt.% and 0.3 ~ 0.5 wt.%, respectively.

Because of the above reasons the composition usually used for the Hall bath is 80-86% Na_3AlF_6, 4-6% CaF_2, 5-10% AlF_3, 3-5% Al_2O_3, 0.3-0.5% MgF_2 and 0.1% LiF (wt.% basis).

Now, it is well known that in order to increase energy efficiency, the composition of the Hall bath will need to be modified. A cryolite solution having lower temperature and higher alumina content at the double solubility limit, higher electrical conductivity, higher interfacial tension and proper density, etc., is the goal.

Phase diagrams show the relationships between liquidus temperature and composition. Although a large amount of work has been done in the past several decades, the real reactions in the Hall cell and interactions between components are still unknown. Thoroughly understanding the phase relationship is useful to appreciate them.

B. Previous Work

Before studying the quaternary system Na_3AlF_6-CaF_2-AlF_3-Al_2O_3, some previous work connected with this quaternary system should be reviewed.

1) Ternary System Na_3AlF_6-CaF_2-AlF_3

Brown and Craig [14] used DTA technique combined with X-ray diffraction analysis, quenching and optical microscopic examination to determine Na_3AlF_6-CaF_2-AlF_3 phase diagram.

The main features are:

a) The system has five compounds, i.e., $NaCaAlF_6$, $Na_5Al_3F_{14}$, $NaCaAl_2F_9$, $CaAlF_5$ and Ca_2AlF_7.

b) The liquidus surface of the Na_3AlF_6-CaF_2-AlF_3 phase diagram is shown in Fig. 4. There are ten invariant points including an eutectic point at 30 mole % Na_3AlF_6, 15 mole % CaF_2, 55 mole % AlF_3 and 680°C.

c) At 561°C, Na_3AlF_6 has a polymorphic transformation. Both α and β Na_3AlF_6 can accommodate $NaCaAlF_6$ in a solid solution.

However, the liquidus temperatures obtained from DTA experiments are approximate values. The accuracy which depends on the instrument used and operator's skill may be ±15°C. In order to get more accurate data, quenching methods and optical microscopic examination are recommended.

2) System Na_3AlF_6-Al_2O_3-CaF_2

Rolin [15] has showed that this phase diagram is a simple eutectic system having a ternary invariant point at 78 wt.% Na_3AlF_6, 17 wt.% CaF_2, 5 wt.% Al_2O_3 and eutectic temperature 927°C (Fig. 5).

3) System Na_3AlF_6-AlF_3-Al_2O_3

Foster [16] studied the cryolite-rich portion of this system and the resulting phase diagram is shown in Fig. 6.

The eutectic boundary curve of Na_3AlF_6-Al_2O_3 shows a gradual decrease in Al_2O_3 content to ternary peritectic composition located at 723°C and 4.4 wt.% Al_2O_3, 28.3 wt.%

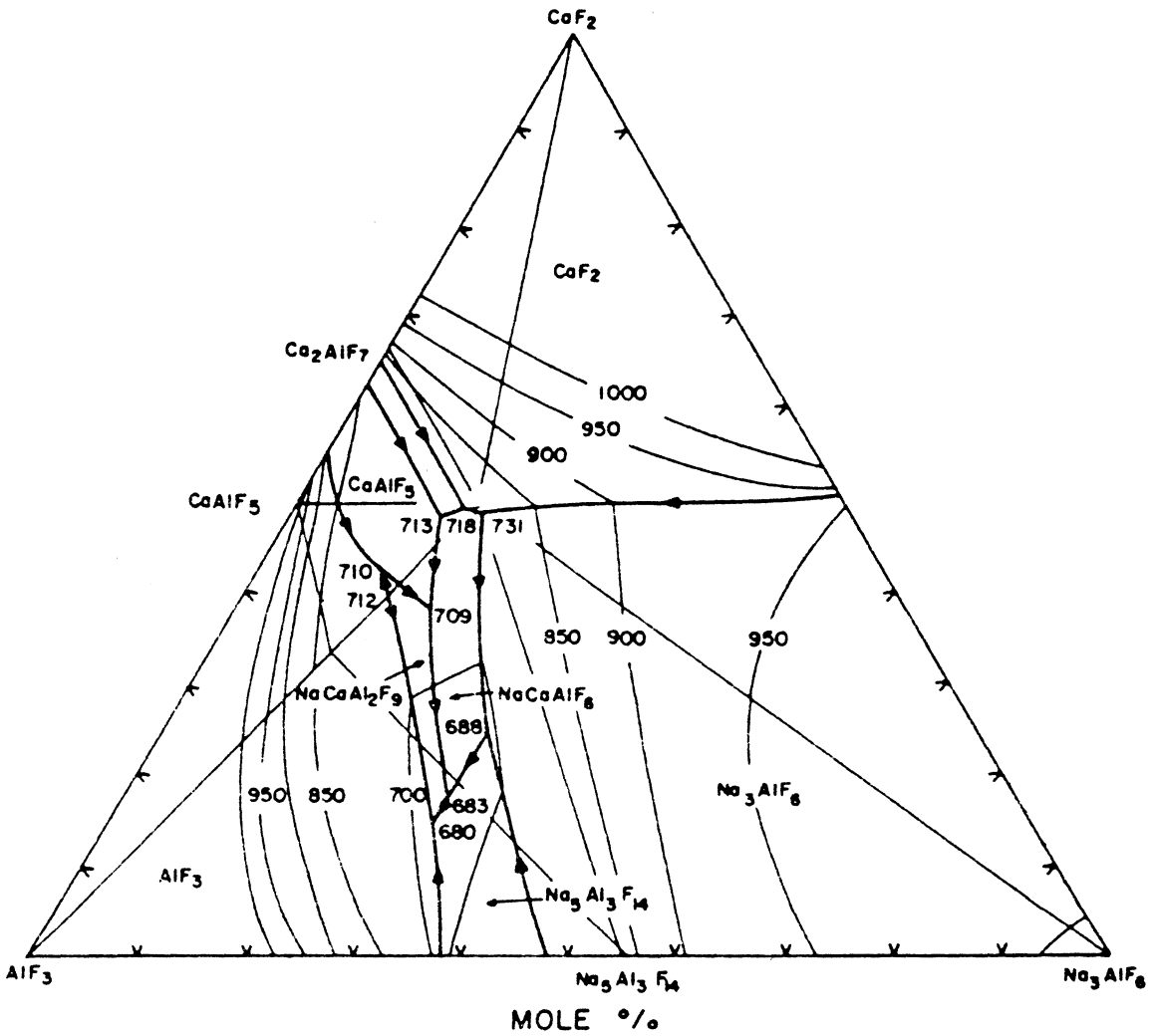

Fig. 4. Liquidus surface of the system Na_3AlF_6-CaF_2-AlF_3.[14]

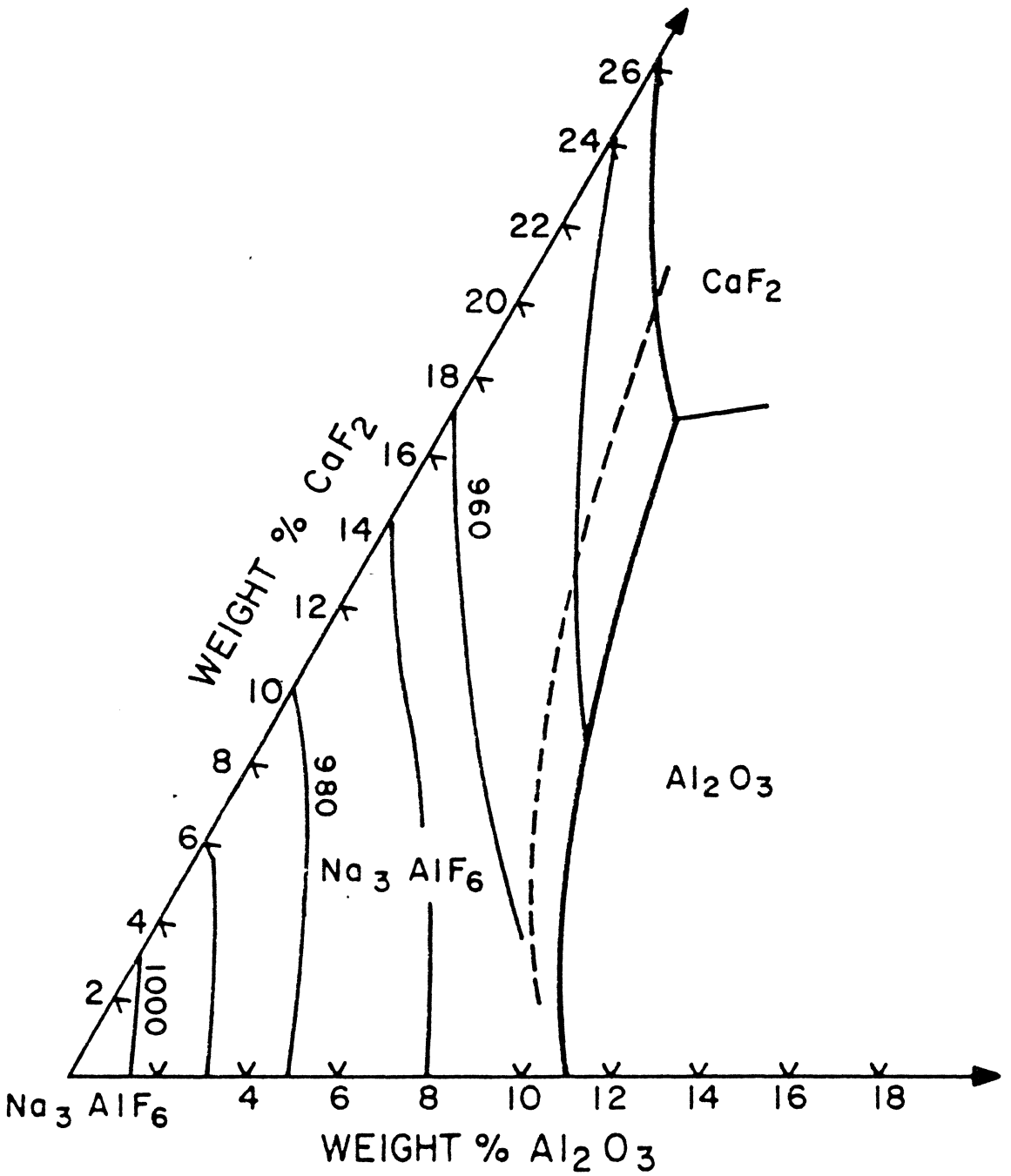

Fig. 5. System Na_3AlF_6-Al_2O_3-CaF_2.[15]

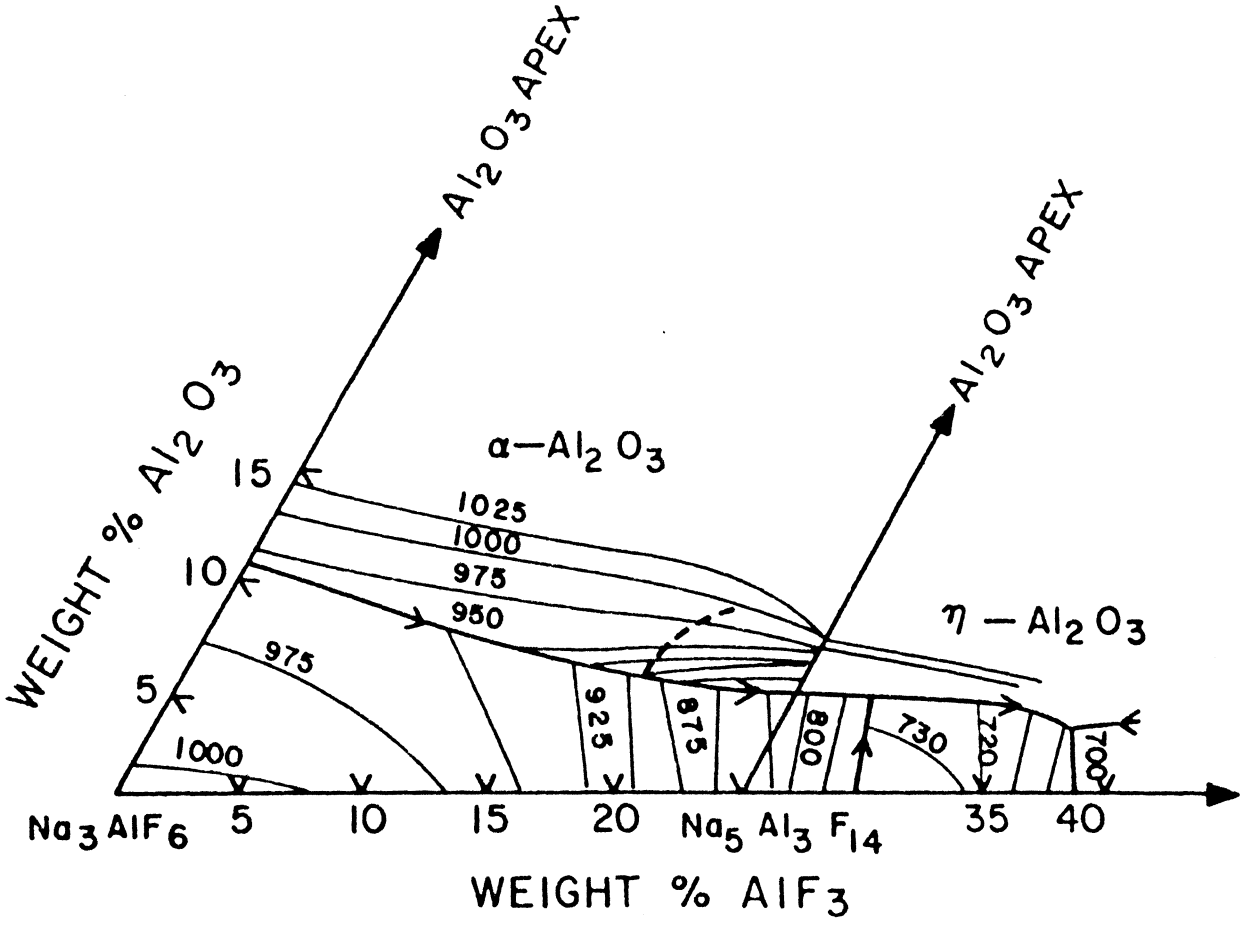

Fig. 6. System Na_3AlF_6-AlF_3-Al_2O_3.[16]

AlF_3, 67.3 wt.% Na_3AlF_6.

A ternary eutectic is located at 59.5 wt.% Na_3AlF_6, 33.3 wt.% AlF_3, 3.2 wt.% Al_2O_3 and 684°C.

Both the Na_3AlF_6-CaF_2-Al_2O_3 and Na_3AlF_6-AlF_3-Al_2O_3 phase diagrams show that increasing the Al_2O_3 content in cryolite solution will lower the cryolite liquidus temperature until the double solubility limit is reached. Beyond this limit, the primary phase is Al_2O_3 and the liquidus temperature increases with increasing alumina content.

4) Quaternary System Na_3AlF_6-CaF_2-AlF_3-Al_2O_3

Abramov et al. [17], Foster [18], Fennerty and Hollingshead [19], Rolin [30], Brown and Craig [14], Brown and Lee [21], Brown and Lei [22], etc. studied this quaternary system. Their findings can be summarized as follows:

a) The entire system can be divided to eight compatibility triangles (Fig. 7).

b) No quaternary compound exists in this system.

c) A quaternary peritectic point exists at 56.7 wt.% Na_3AlF_6, 30.2 wt.% AlF_3, 8.5 wt.% CaF_2, 4.6 wt.% Al_2O_3 and 685°C. Also, a quaternary eutectic point exists at 665°C.

d) Over certain composition ranges (2∿5 wt.% Al_2O_3, CR = 1.1 ∿ 1.51, 7∿9 wt.% CaF_2), the liquidis temperature decreases with increasing Al_2O_3, AlF_3 and CaF_2.

e) The addition of $NaCaAlF_6$(in other words the addition of CaF_2 and AlF_3) decreases the liquidus temperature of the system Na_3AlF_6-Al_2O_3. Meanwhile, it shifts the eutectic

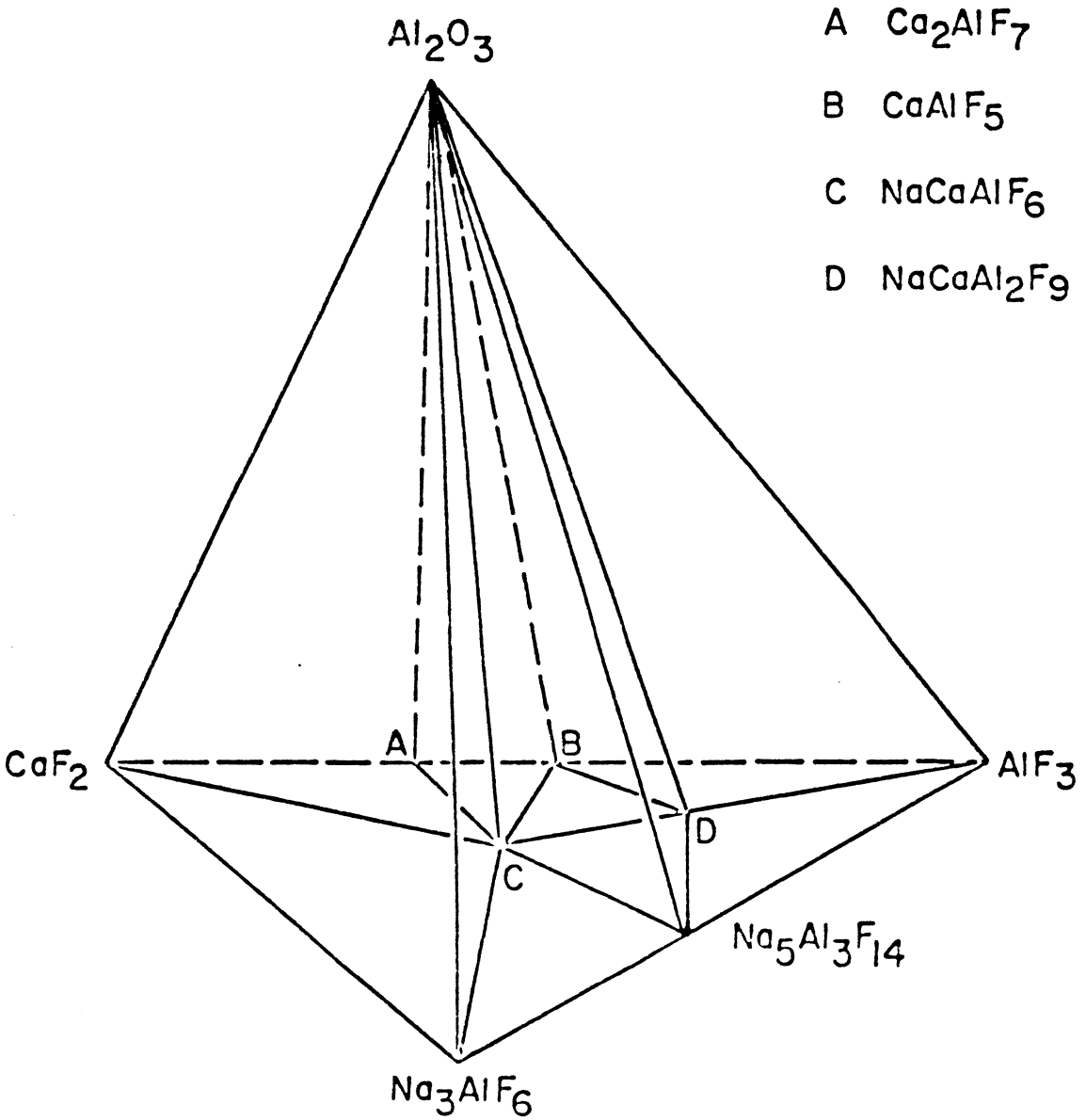

Fig. 7. Sub-solidus compatibility relationships in the quaternary system Na_3AlF_6-AlF_3-CaF_2-Al_2O_3. [14]

composition of system Na_3AlF_6-Al_2O_3 to lower alumina content (Fig. 8).

(f) In order to calculate the liquidus temperature of cryolite-rich portion of this quaternary system, Dewing [23] used an expression in the form of

$$t = t_o + \sum_{i.j.n} a_i (X_j)^n \qquad (6)$$

where t - the liquidus temperature

t_o - a constant

a_i - coefficient

X_j - the weight percentage of component j

n - positive integer

This expression may be applied to the region $CaF_2 \leq 12$ wt.% and $AlF_3 \leq 16.67$ wt.%.

Richard [24] adopted another expression

$$t = 998.7 - 1.06\, X_{AlF_3} - 5.4\, X_{Al_2O_3} - 1.01\, X_{CaF_2} - 4\, X_{Li_3AlF_6} \qquad (7)$$

where X_{AlF_3}, $X_{Al_2O_3}$ . . . . are weight percentages of compositions, respectively. This expression may be applied to the region Al_2O_3 2.5-6 wt.%, CaF_2 3-6 wt.% and Li_3AlF_6 0.5 wt.%, with cryolite ratio in the range of 1.25 $\sim$ 1.4.

Both of these expressions are based on the assumption that the liquidus temperatures represent some linear combination of the effect of individual components or their n powers.

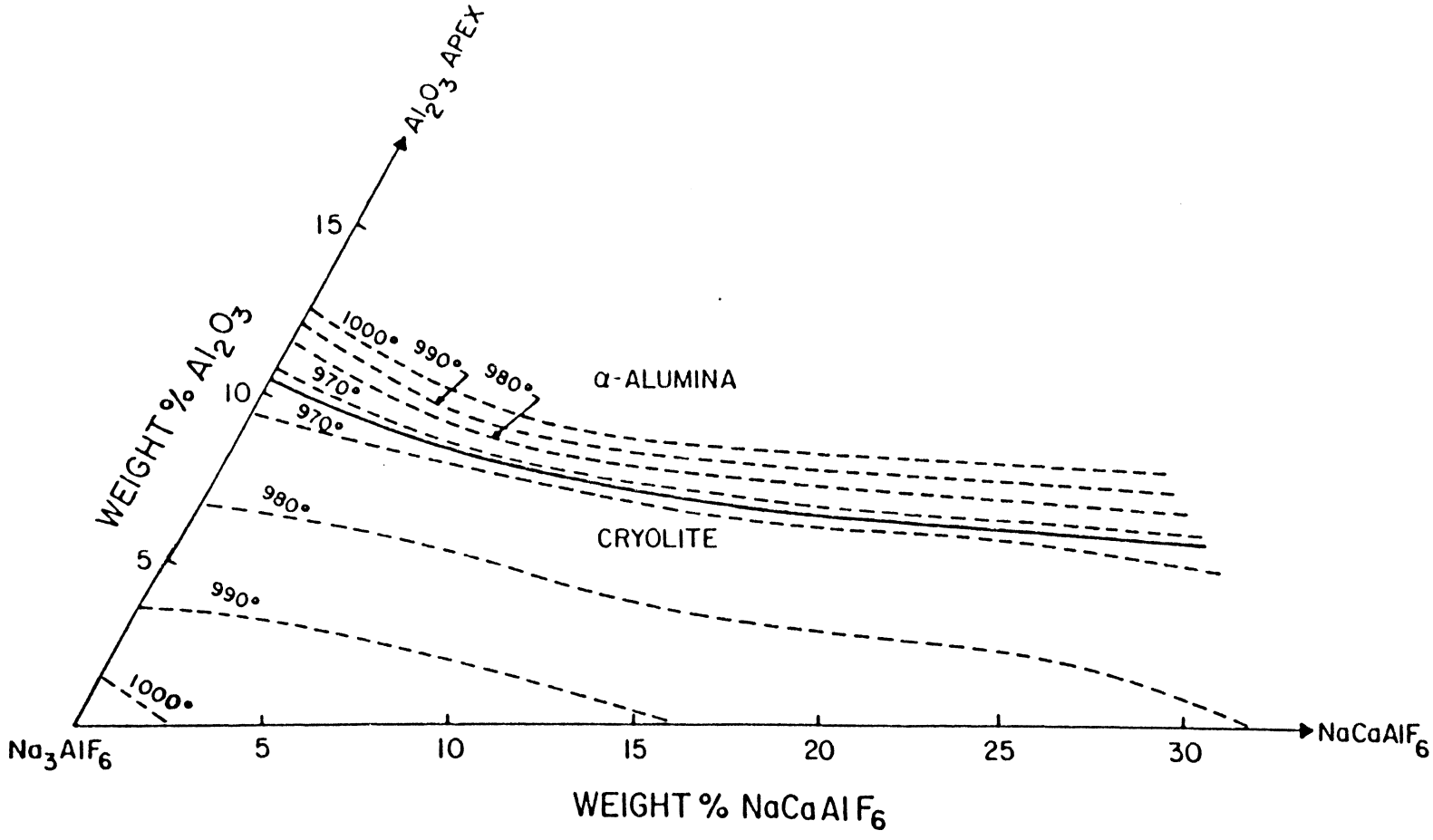

Fig. 8. Liquidus surface of the cryolite-rich portion of the system Na_3AlF_6-$NaCaAlF_6$-Al_2O_3.[22]

C. Objectives of This Study

This study, sponsored by ALCOA, is a continuation of the phase equilibria studies which have been conducted for several years in the Department of Materials Engineering at Virginia Polytechnic Institute and State University. The purposes of this work are

1) Precisely measuring the liquidus temperatures of the selected compositions of the cryolite-rich portion in the Na_3AlF_6-CaF_2-AlF_3 ternary system (Fig. 9) and map the isotherms of the region.

2) Determining the pseudo binary liquidus diagrams of AlF_3 and CaF_2-containing cryolite solution - Al_2O_3 systems. (Compositions 6, 7, 8, 9, 10, 11, 13, 15, 17, and 19), and thereafter, getting the alumina contents and temperatures at the double solubility limit for different AlF_3 and CaF_2 contents in order to offer some information for deciding a reasonable compositional range and the operating temperature of the Hall cell.

The research program was carried out by the quenching method complemented with DTA and optical microscopic examination.

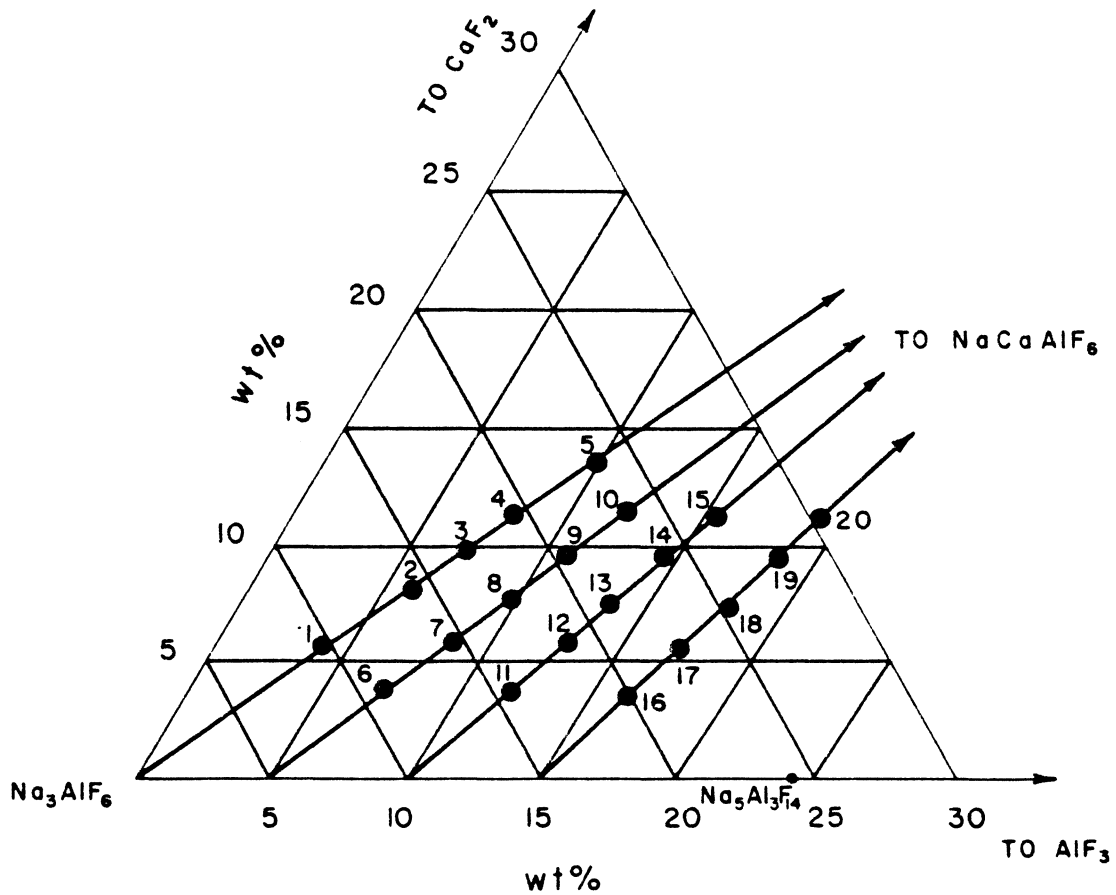

Fig. 9. The selected compositions used to map the liquidus surface of the system Na_3AlF_6-CaF_2-AlF_3.

II. EXPERIMENTAL PROCEDURES

1) Sample Preparation

a) Materials

The raw materials used in this study were: cryolite (Na_3AlF_6) - natural Greenland cryolite*, anhydrous aluminum fluoride (AlF_3) containing 1.93% Al_2O_3**, reagent-grade calcium fluoride (CaF_2)+, anhydrous alumina‡.

b) All powders were calcined in a muffle furnace at 200°C for 24 hrs.

c) According to specified composition, the calcined powders were weighed on a analytical balance§ having an accuracy of 0.0001 g.

d) The powders were ground and mixed with acetone in a glass mortar.

e) After the acetone was allowed to volatilize, the mixed powder was recalcined at 200°C for 24 hrs.

f) The recalcined powder was ground and encapsulated into platinum tubes, 3 mm O.D. and 10 mm in length.

g) The platinum tube was sealed.

h) The sealed sample was heat-treated at 30-50°C above the estimated liquidus temperature (at least 950°C) for 1/2

---

*Na_3AlF_6, provided by ALCOA, Pittsburgh, PA.
**AlF_3, provided by ALCOA, Pittsburgh, PA.
+Purchased from Fisher Scientific Company, Fair Lawn, N.J.
‡Purchased from Fisher Scientific Company, Fair Lawn, N.J.
§Manufactured by Preiser Scientific Inc.

hr, and then cooled slowly to room temperature. This was done in order to make this sample homogeneous and to check if there was any leakage at the sealed ends of the tube. If the sample tube swelled and there was no white powder on the outside of the tube (from condensation of escaped volatiles) after heat treated, then the sample was used for running DTA and quenching.

2) DTA

Differential thermal analysis is a dynamics method of examining phase transformation.

To run DTA, a sample which is used to measure the liquidus temperature of specified composition and a reference material which is used to check temperature readings are put side by side in a special furnace.* In this study, both the sample and the reference material were heat-treated platinum tubes filled with powders of a specified composition studied and pure quartz, respectively. The reason for using quartz is as follows: The transformation temperature of low quartz to high quartz is 573°C, a defined temperature which can be used to check all the temperature readings in this study, and there is no further phase transformation in ordinary condition until 1470°C which is the transformation temperature for high quartz to cristobalite.

---

*A 1600°F furnace module (910 Differential Scanning Calorimeter) equipped with a DuPont 990 Differential thermal analyzer.

Two thermocouples are inserted in the furnace. They are attached to the two platinum tubes, respectively. When the furnace is heated to high temperature and then cooled at a specified rate (5°C/min) the temperature difference of the two thermocouples is recorded. If no phase transformation occurs in the sample or in quartz, there is no temperature difference between the two thermocouples. Once the sample (or quartz) undergoes a phase transformation, there exists a transient temperature difference between the sample and quartz due to the enthalpy change of the sample (or quartz), which can be revealed as a peak of emf difference on a recorded paper. From the position of this peak, the temperature of the phase transformation can be obtained.

Both peaks occurring in heating curve or cooling curve on the recorded paper can be used to obtain the temperature of phase transformation. In this study, peaks occurring in heating curve rather than cooling curve are used because the temperature of phase transformation can be seriously influenced by supercooling [14].

3) Quenching

After obtaining an approximate liquidus temperature from DTA data, the next procedure is to quench the sample.

The heat treated sample was suspended in a tube furnace* by a nickel wire inserted through a ceramic thermocouple tube.

*A Tem-Pres water cooled vertical tube furnace, incorporated by Penn State University.

A pt/pt-10 Rh thermocouple protruded from another two holes in the same ceramic tube with the sample some 2-3 mm from the welded junction. The tube furnace was then heated to 30-40°C above the quenching temperature estimated by DTA data and held at that temperature for 20-30 min. After that, the sample was cooled slowly to the quenching temperature (about 1 ∿ 1.5°C/min) and held at the quenching temperature for 3 hrs. Finally, the sample was quenched into a pot with cold water (0-3°C).

The furnace temperature was monitored by an pt/pt-10 Rh thermocouple and millivolt potentiometer**. The pt/pt-10 Rh thermocouple was calibrated by a standard pt/pt-10 Rh thermocouple which was calibrated by National Bureau of Standard. The range of temperature fluctuation was ±2°C during experimentation and calibration.

If the quenching temperature was above the liquidus temperature, after quenching, the microstructure of the sample should consist of a glassy phase. If the quenching temperature is below liquidus temperature, the microstructure of the quenched sample should consist of glassy phase and primary crystals. Therefore, accurate determination of the liquidus temperature may be obtained by observing the microstructure of the quenched sample.

**Cat. 8686, manufactured by Leeds and Northrup Co., Philadelphia.

4) Optical Microscopic Examination

The quenched platinum tube was opened and the powder within the tube was removed, crushed and mixed in an agate mortar. Material taken from mixed powder was homogeneously spread on a glass slide and viewed under an optical microscope with transmitted white light*.

The glassy phase is an opaque phase with an irregular shape.

In this study, the primary crystal was recognized by its characteristic, i.e. shape, transparency, cleavage and refractive index (Table 1) [25,26]. Therefore chiolite could be easily recognized from cryolite and corundum under the microscope (Fig. 10). Cryolite and corundum were distinguished by using the Becké line method with a suitable immersion oil having a refractive index between 1.338 and 1.75. Figure 11 and Fig. 12 show the microstructure of glassy phase, cryolite and corundum.

5) X-Ray Powder Diffraction

In order to identify the primary phase determined by optical microscopy, x-ray powder diffraction experiments for compositions 12, 15, 17, 19 and 85% Na_3AlF_6 - 15% AlF_3

---

*A Reichert MeF2 universal camera microscope equipped with transmitted and reflected light sources, polarizers, analyzers and a Bertrand lens.

TABLE 1. THE CHARACTERISTIC OF CRYOLITE, CHIOLITE AND CORUNDUM

Item	Cryolite (Na_3AlF_6)	Chiolite ($Na_5Al_3F_{14}$)	Corundum (α-Al_2O_3)
Crystal System	Monoclinic	Tetragonal	Hexagonal
Point Group	2/m	$^4/_m{}^2/_m{}^2/_m$	$\bar{3}$ 2/m
Space Group	P $2_1/n$	P 4/mnC	R $\bar{3}$c
Lattice Constants	a=5.40 Kx b=5.60 Kx c=7.78 Kx β=90°11'	a=7.005 Kx c=10.39 Kx	a=4.751 Kx c=12.97 Kx
3 Strongest Diffraction Lines	1.941 Kx (100) 2.747 Kx (95) 3.883 Kx (60)	2.91 Kx (100) 5.18 Kx (80) 2.32 Kx (70)	2.085 Kx (100) 2.552 Kx (90) 1.601 Kx (80)
Optical Constants	α=1.3376 β=1.3377 γ=1.3387	ω=1.3486 ε=1.3424	ω=1.7653-1.7760 ε=1.7573-1.7677
Hardness	2 1/2	3 1/2-4	9
Density (g/cc)	2.97 (meas.) 2.963 (calc.)	2.998 (meas.) 2.989 (calc.)	4.0-4.1 (meas.) 3.987 (calc.)
Cleavage	none	{001} perfect {011} distinct	none
Fracture	uneven brittle		conchoidal to uneven brittle

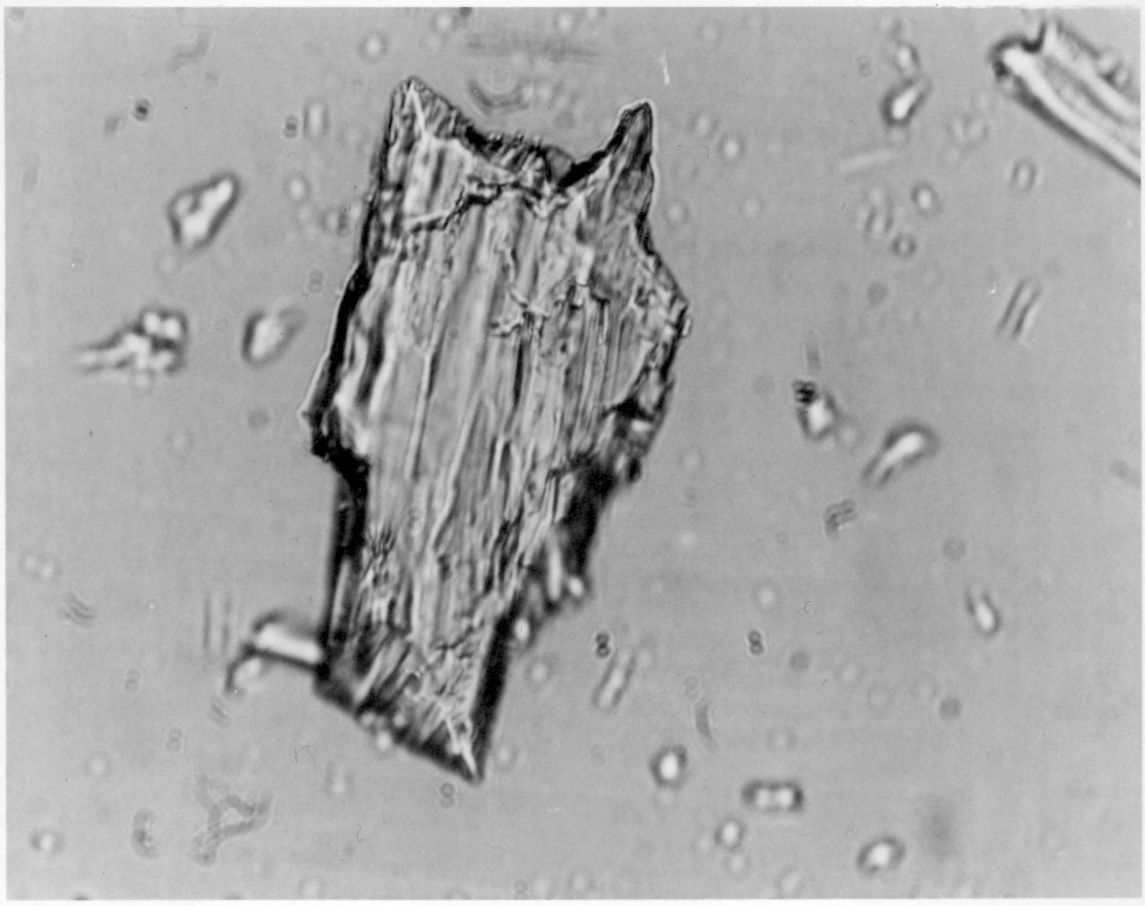

Fig. 10. Optical micrograph of chiolite ($Na_5Al_3F_{14}$).
Sample: Natural Greenland chiolite mineral.

Refractive index of oil	1.3919
Microstructure	chiolite
Magnification	234x

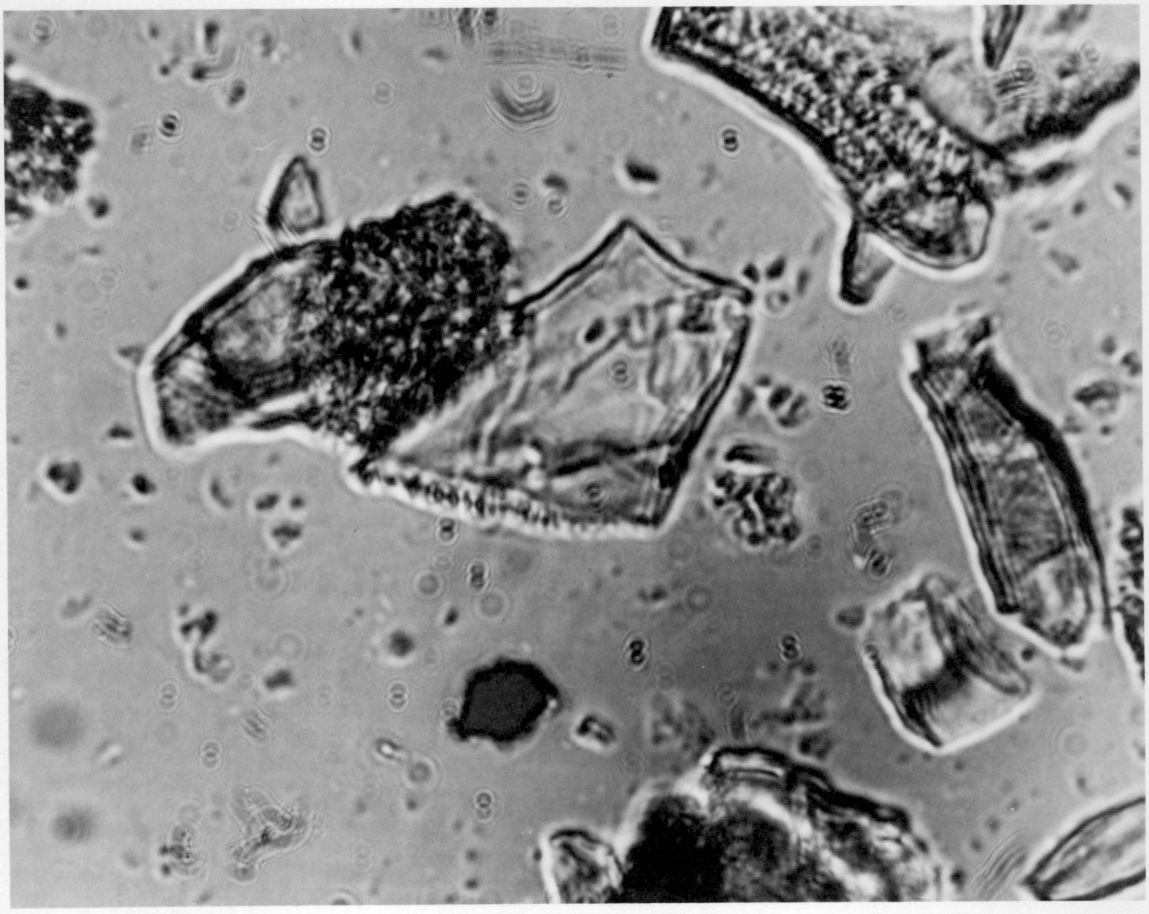

Fig. 11. Optical micrograph of quenched sample.

Sample: 84.43% Na_3AlF_6 3.83% CaF_2 11.51% AlF_3 0.23% Al_2O_3	quenched from 940°C
Refractive index of oil	1.3919
Microstructure	Glassy phase + Primary crystal of cryolite
Magnification	584x

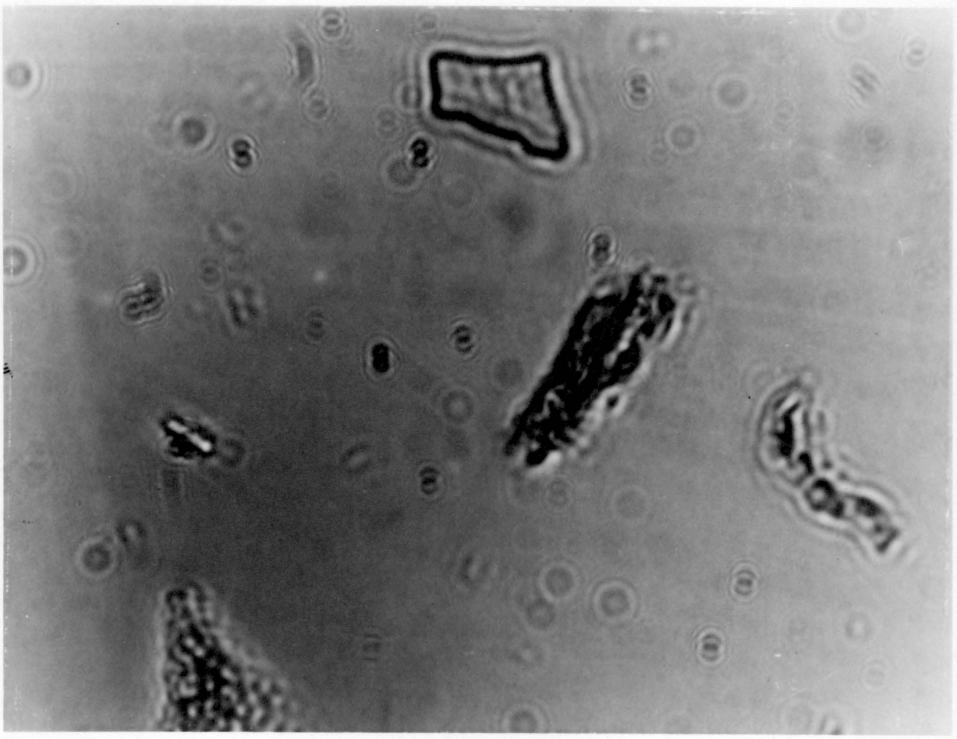

Fig. 12. Optical micrograph of quenched sample.
Sample: 72.18% Na_3AlF_6 10.79% CaF_2 11.03% AlF_3
6.0% Al_2O_3 quenched from 969°C

Refractive index of oil	1.3919
Microstructure	Glassy phase + Primary crystal of corundum
Magnification	864x

were done by using a x-ray powder diffractometer* and nickel filtered CuK_{α} radiation.

*Nerolco X-ray unit. Model 12100115/9, Philips Electronic Instruments.

III. RESULTS AND DISCUSSION

1) Liquidus Surface of Cryolite-Rich Portion of Na_3AlF_6-CaF_2-AlF_3 Ternary System

Data for quenched samples of compositions 11-20 (shown in Fig. 9) were shown in Fig. 13 and Fig. 14. All the liquidus temperatures for compositions 1-20 of the cryolite-rich portion of ternary system Na_3AlF_6-CaF_2-AlF_3 are listed in Table 2. The isotherms of the liquidus surface based on the data of Table 2 are plotted in Fig. 15.

a) From Fig. 15, it may be seen that for compositions of the cryolite-rich portion, the primary phase identified by using optical microscopy is cryolite. As indicated by Brown and Craig [14] and Brown and Lee [21], this primary phase is a cryolite solid solution rather than pure cryolite.

b) The liquidus temperatures decrease with increasing CaF_2 or AlF_3 content.

c) There exist inflections in the isotherms. The reason for this may be understood by referring to the Na_3AlF_6-AlF_3 phase diagram (Fig. 16) [27]. The slope of the liquidus curve increases with increasing the AlF_3 content, and at the peritectic temperature (741°C), the AlF_3 solubility is 30 wt.% AlF_3. However, the liquidus curve of Na_3AlF_6-CaF_2 phase diagram (Fig. 17) [28] remains linear until the eutectic (945.5°C, 50 wt.% CaF_2, i.e., 27.1% CaF_2) and the slope of the liquidus curve is small. As a result,

TABLE 2. THE LIQUIDUS TEMPERATURES OF THE SELECTED COMPOSITIONS OF CRYOLITE-RICH PORTION OF THE SYSTEM Na_3AlF_6-CaF_2-AlF_3

Composition	Theoretical (Wt.%)			Batch (Wt.%)				Measured Temperatures* (°C)	
	Na_3AlF_6	$NaCaAlF_6$	AlF_3	Na_3AlF_6	CaF_2	AlF_3	Al_2O_3	Liquid + Solid	Liquid
1	85.0	15.0	-	90.14	5.74	4.04	0.08	993.4	994.9
2	80.0	20.0	-	86.86	7.63	5.40	0.11	987.1	988.7
3	75.0	25.0	-	83.57	9.57	6.73	0.13	979.9	981.4
4	70.0	30.0	-	80.29	11.48	8.07	0.16	970.0	971.9
5	65.0	35.0	-	77.0	13.39	9.42	0.19	961.7	964.1
6	85.0	10.0	4.5	88.93	3.83	7.10	0.14	991.5	993.5
7	80.75	15.0	4.25	85.89	5.74	8.20	0.17	984.5	986.5
8	76.0	20.0	4.0	82.87	7.63	9.30	0.20	980.5	981.5
9	71.25	25.0	3.75	79.82	9.57	10.40	0.21	969.0	971.0
10	66.5	30.0	3.5	76.79	11.48	11.49	0.23	959.0	961.0
11	81.0	10.0	9.0	84.43	3.83	11.51	0.23	954.5	956.5
12	76.5	15.0	8.5	81.65	5.74	12.37	0.24	945.5	948.5
13	72.0	15.0	8.0	78.86	7.66	13.22	0.26	938.5	940.5
14	67.5	25.0	7.5	76.08	9.57	14.07	0.28	932.5	935.5
15	63.0	30.0	7.0	73.29	11.49	14.93	0.29	927.5	929.5
16	76.5	10.0	13.5	79.93	3.83	15.93	0.31	909	911
17	72.25	15.0	12.75	77.40	5.74	16.53	0.33	896.5	897.5
18	68.0	20.0	12.0	74.86	7.66	17.14	0.34	883	884
19	63.75	25.0	11.25	72.33	9.57	17.75	0.35	874	875
20	59.5	30.0	10.5	69.79	11.49	18.36	0.36	870	872

*The liquidus temperatures for compositions 1-5 were determined by Lee [21].

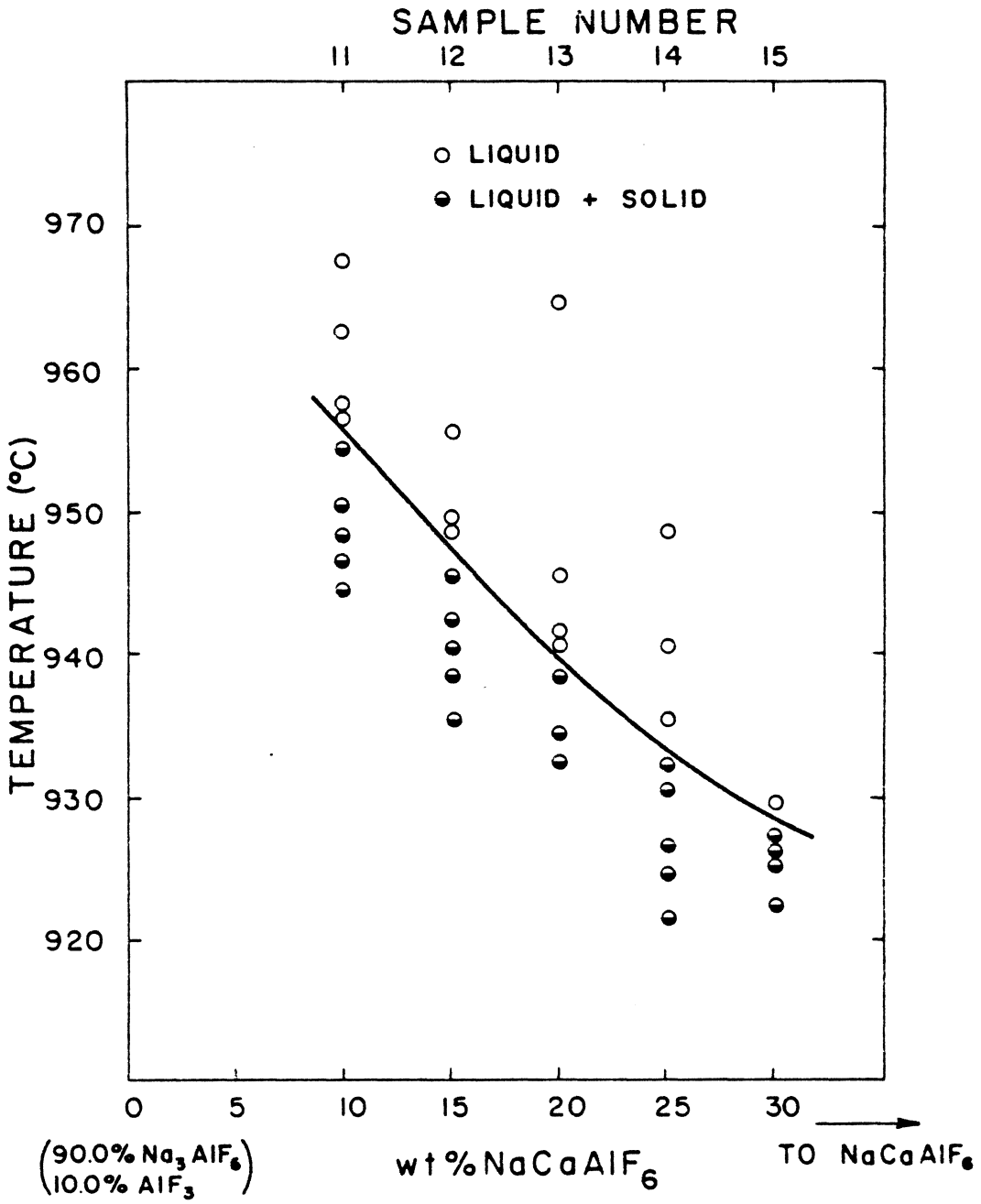

Fig. 13. Liquidus temperature for the join 90 Na_3AlF_6/10 AlF_3-$NaCaAlF_6$.

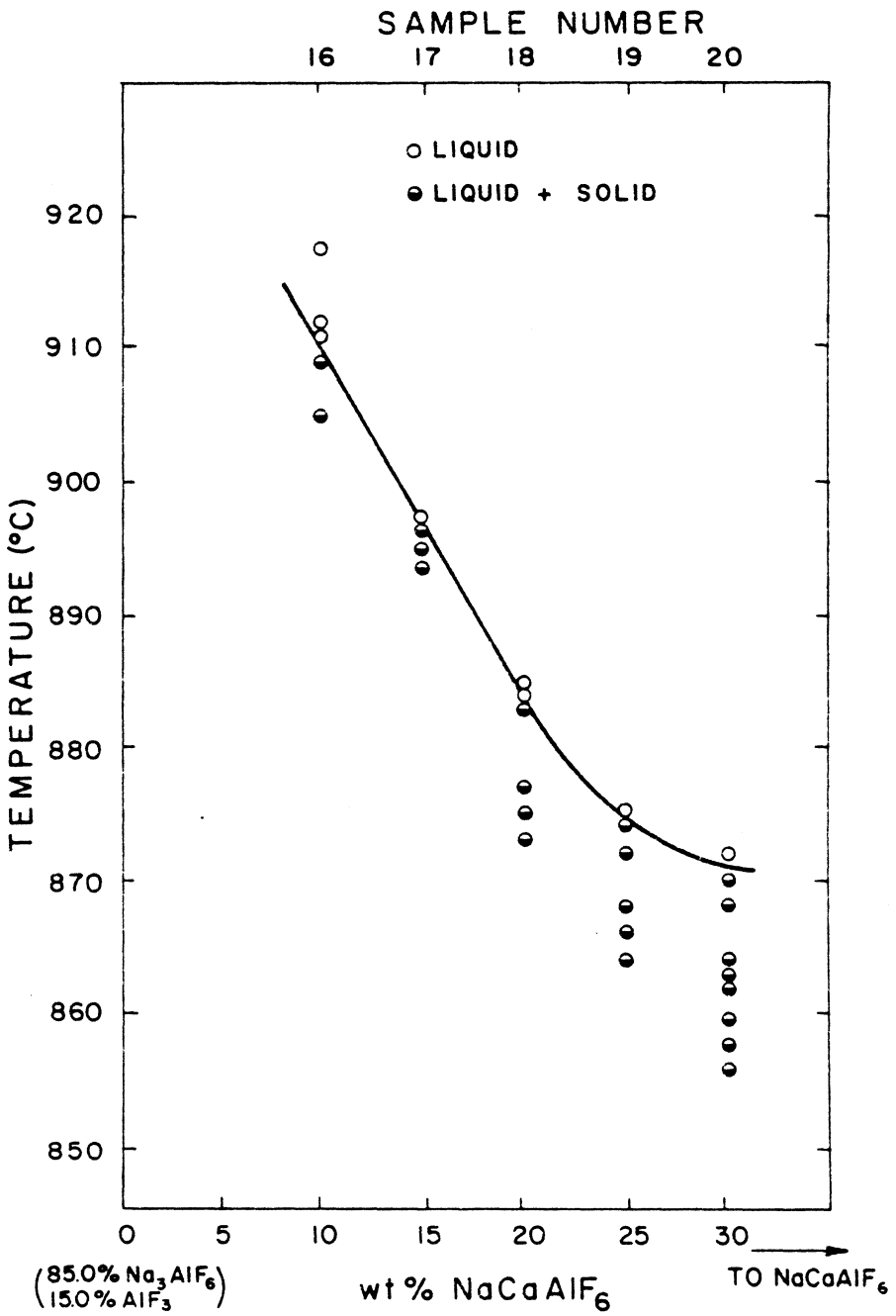

Fig. 14. Liquidus temperature for the join 85 Na_3AlF_6/15 AlF_3-$NaCaAlF_6$.

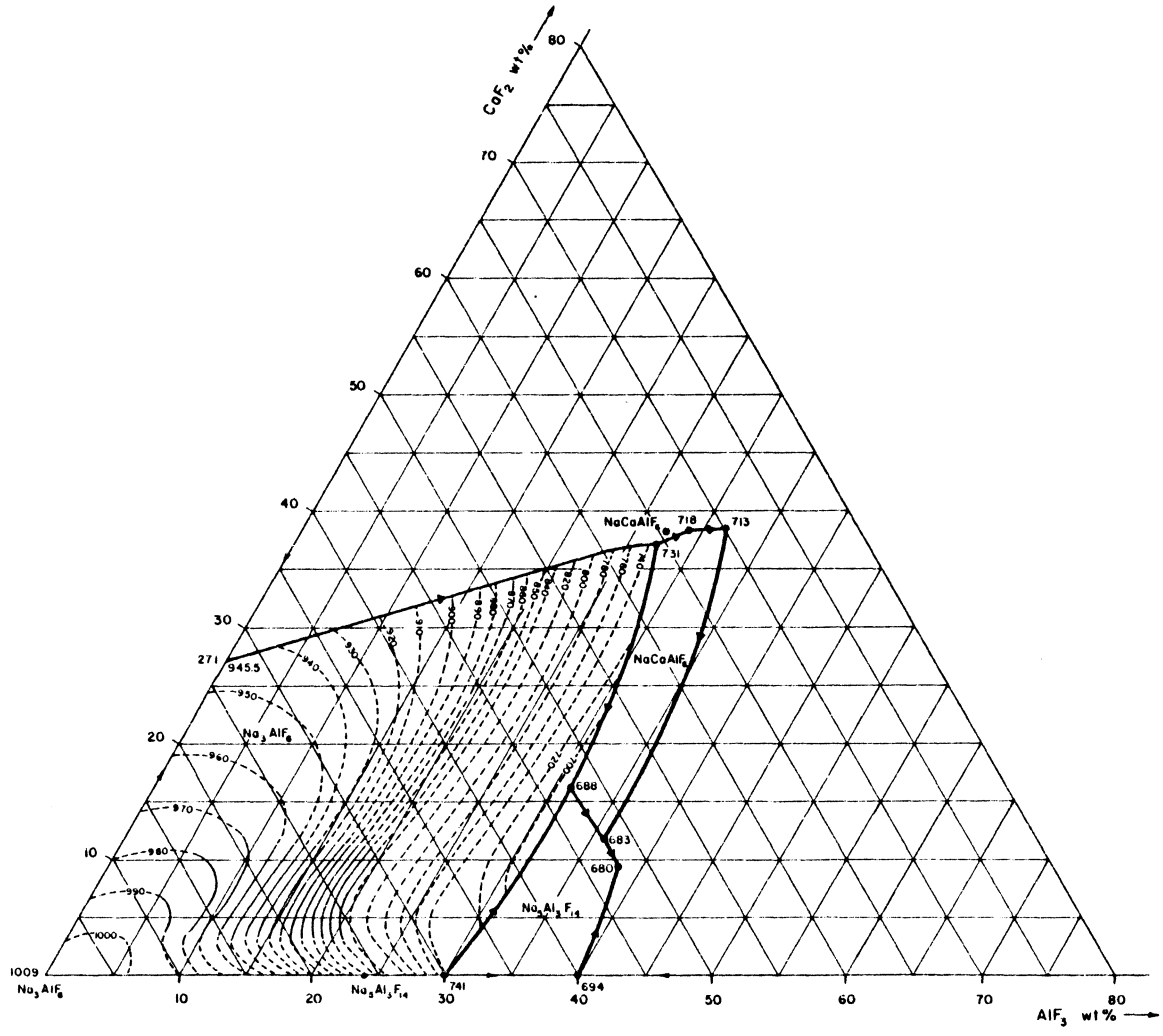

Fig. 15. Isotherms for cryolite-rich portion of the ternary system Na_3AlF_6-CaF_2-AlF_3.

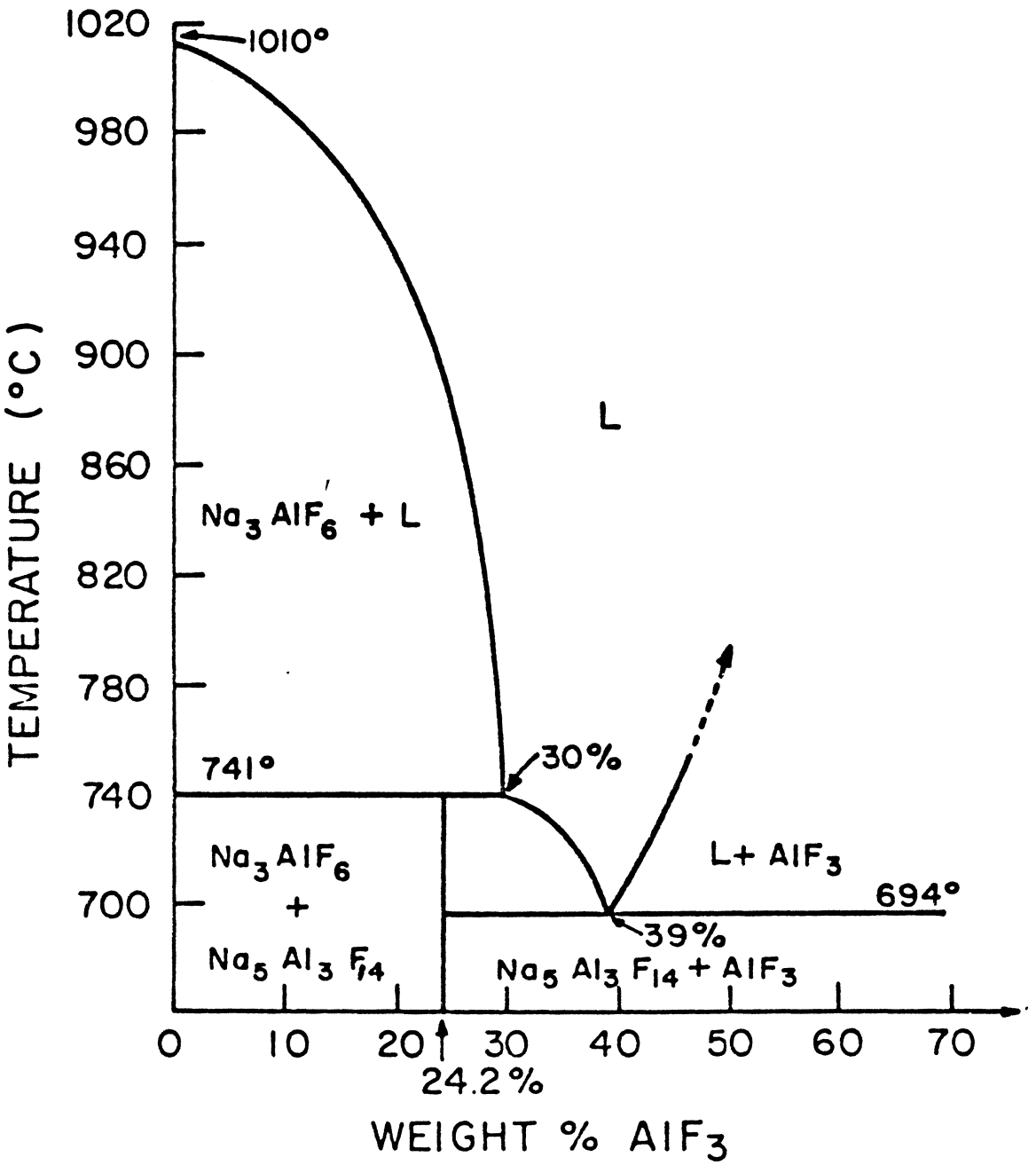

Fig. 16. System Na_3AlF_6-AlF_3.[27]

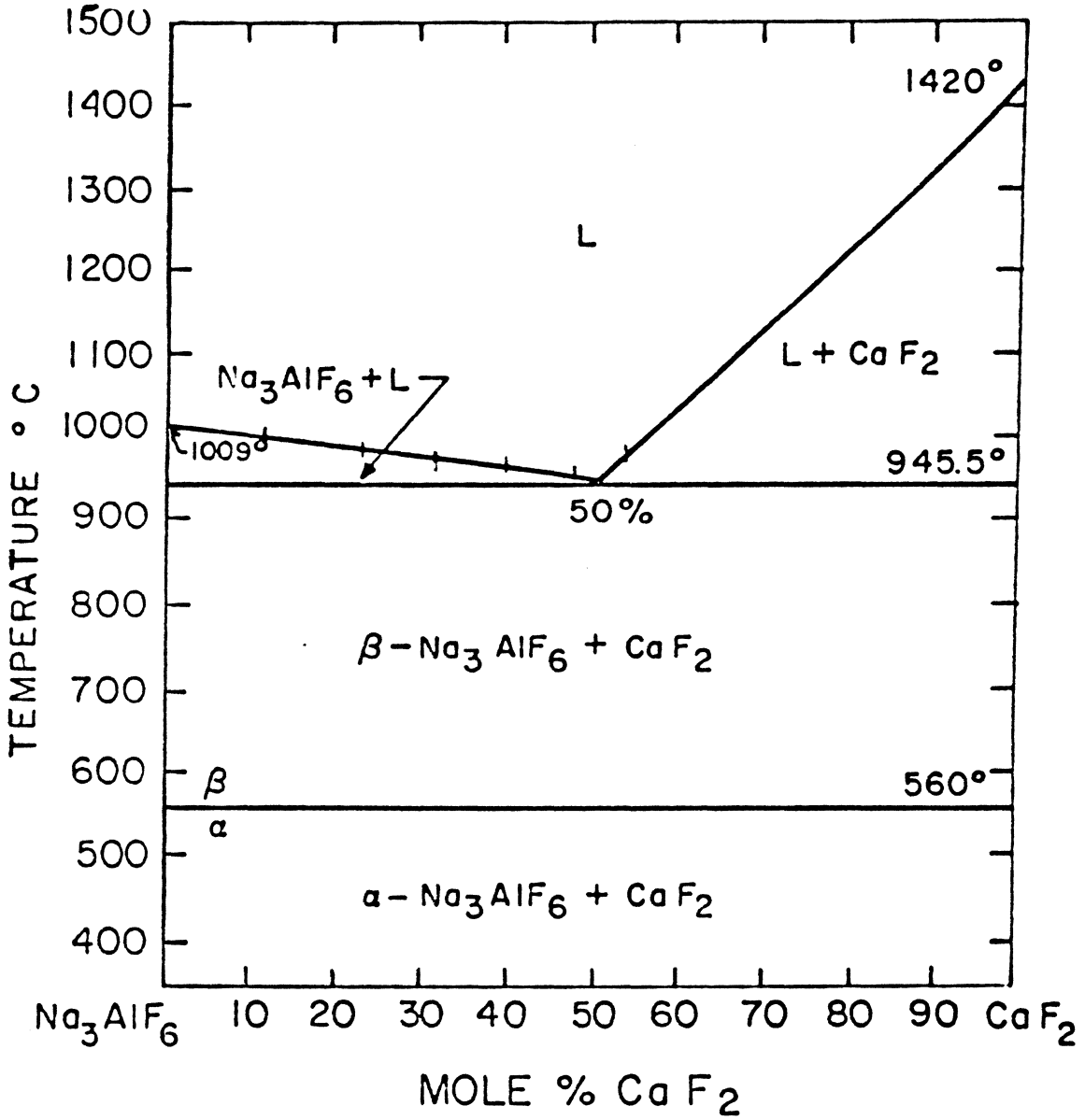

Fig. 17. System Na_3AlF_6-CaF_2.[28]

any surface which connects the two binary liquidus curves may show inflection points.

2) The Alumina Solubilities of Selected Compositions

The liquidus temperatures of different Al_2O_3 additions (0 ~ 8 wt.% Al_2O_3) to selected compositions in the Na_3AlF_6-CaF_2-AlF_3 ternary system are listed in Table 3. For all ten compositions, pseudo-binary phase diagram shown in Fig. 18, 19 and 20 were obtained by using the data listed in Table 3.

The alumina solubilities of compositions 6-10 (their base compositions which can be seen in Fig. 9 lie along a single join) are shown in Fig. 18 (a) ~ (e). The double solutility limit (i.e. eutectic point) of each composition was obtained from these figures. All the eutectic temperatures and compositions were collected in Fig. 18 (f) which shows the temperatures and alumina contents at the double solubility limit for the join $NaCaAlF_6$-95 Na_3AlF_6/5 AlF_3. Similarly, Fig. 19 and Fig. 20 show the temperatures and alumina contents of compositions on the join $NaCaAlF_6$ - 90 Na_3AlF_6/10 AlF_3 and $NaCaAlF_6$ - 85 Na_3AlF_6/15 AlF_3, respectively.

The results from these figures are:

a) Each of these pseudo binary phase diagram is an eutectic type as described by Brown and Lee [21], Dewing [11] and Foster [10].

TABLE 3. THE LIQUIDUS TEMPERATURES OF DIFFERENT Al_2O_3 CONTENTS OF TEN SELECTED COMPOSITIONS

Composition*	Theoretical (Wt.%)				Batch (Wt.%)				Measured Temperatures (°C)	
	Na_3AlF_6	$NaCaAlF_6$	AlF_3	Al_2O_3	Na_3AlF_6	CaF_2	AlF_3	Al_2O_3	Liquid+ Solid	Liquid
6-0	85.0	10	4.5	-	88.93	3.83	7.10	0.14	991.5**	993.5
6-2	83.79	9.8	4.41	2.0	87.15	3.75	7.10	2.0	982.5**	984.5
6-4	82.08	9.6	4.32	4.0	85.38	3.67	6.95	4.0	971.0**	973.0
6-6	80.37	9.4	4.23	6.0	83.59	3.60	6.81	6.0	960.0***	961.5
6-7	79.515	9.3	4.185	7.0	82.70	3.56	6.74	7.0	969.0***	971.0
6-8	78.66	9.2	4.14	8.0	81.82	3.52	6.66	8.0	1000.5	1002.5
7-0	80.75	15	4.25	-	85.89	5.74	8.20	0.17	984.5**	986.5
7-2	79.135	14.7	4.165	2.0	84.17	5.63	8.20	2.0	976.0**	978.5
7-4	77.52	14.4	4.08	4.0	82.46	5.51	8.03	4.0	966.0***	968.0
7-6	75.905	14.1	3.995	6.0	80.74	5.40	7.86	6.0	959.0***	961.0
7-7	75.098	13.95	3.952	7.0	79.88	5.34	7.78	7.0	988.5***	990.5
7-8	74.29	13.8	3.91	8.0	79.02	5.28	7.70	8.0	1017.5	1019.5
8-0	76.0	20	4.0	0	82.87	7.63	9.30	0.20	980.5**	981.5
8-2	74.48	19.6	3.92	2	81.20	7.50	9.30	2.0	970.0**	971.5
8-4	72.96	19.2	3.84	4	79.54	7.35	9.11	4.0	962.0***	962.0
8-6	71.44	18.8	3.76	6	77.89	7.19	8.92	6.0	970.0***	972.0
8-7	70.68	18.6	3.72	7	77.06	7.12	8.82	7.0	999.5	1001.5

*In this item, the first numbers are the composition numbers shown in Fig. 9, and the second numbers are given as the Al_2O_3 contents.

**Cryolite + liquid.

***Corundum + liquid.

TABLE 3. (Continued)

Composition*	Theoretical (Wt.%)				Batch (Wt.%)				Measured Temperatures (C)	
	Na_3AlF_6	$NaCaAlF_6$	AlF_3	Al_2O_3	Na_3AlF_6	CaF_2	AlF_3	Al_2O_3	Liquid + Solid	Liquid
9-0	71.25	25	3.75	-	79.82	9.57	10.40	0.21	969.0**	971.0
9-2	69.825	24.5	3.675	2.0	78.23	9.38	10.40	2.0	959.0**	961.0
9-4	68.4	24	3.6	4.0	76.63	9.18	10.19	4.0	950.0***	952.0
9-6	66.975	23.5	3.525	6.0	75.04	8.99	9.97	6.0	968.0***	970.0
9-7	66.263	23	3.487	7.0	74.23	8.90	9.87	7.0	997.5	999.5
10-0	66.5	30	3.5	-	76.79	11.48	11.50	0.23	959.0**	961.0
10-1	65.835	29.7	3.465	1.0	76.02	11.37	11.61	1.0	954.0**	956.0
10-2	65.17	29.4	3.43	2.0	75.25	11.25	11.50	2.0	949.0***	951.0
10-4	63.84	28.8	3.36	4.0	73.72	11.02	11.26	4.0	940.0***	942.0
10-6	62.41	28.2	3.29	6.0	72.18	10.79	11.03	6.0	999.5	1001.5
11-0	81.0	10.0	9.0	-	84.43	3.83	11.51	0.23	954.5**	956.5
11-2	79.38	9.8	8.82	2.0	82.74	3.75	11.51	2.0	944.5**	946.5
11-4	77.76	9.6	8.64	4.0	81.06	3.67	11.27	4.0	933.5***	935.5
11-6	76.14	9.4	8.46	6.0	79.36	3.60	11.04	6.0	959.5***	961.5
11-7	75.33	9.3	8.37	7.0	78.52	3.56	10.92	7.0	989.0	991.0
13-0	72.0	20.0	8.0	-	78.86	7.66	13.22	0.26	938.5**	940.5
13-2	70.56	19.6	7.84	2.0	77.28	7.50	13.22	2.0	928.5**	930.5
13-4	69.12	19.2	7.68	4.0	75.70	7.35	12.95	4.0	917.0***	919.0
13-6	67.68	18.8	7.52	6.0	74.13	7.19	12.68	6.0	942.5***	945.5
13-7	66.96	18.6	7.44	7.0	73.34	7.12	12.54	7.0	974.5	974.5

TABLE 3. (Continued)

Composition*	Theoretical (Wt.%)				Batch (Wt.%)				Measured Temperatures (°C)	
	Na_3AlF_6	$NaCaAlF_6$	AlF_3	Al_2O_3	Na_3AlF_6	CaF_2	AlF_3	Al_2O_3	Liquid + Solid	Liquid
15.0	63.0	30.0	7.0	-	73.29	11.49	14.93	0.29	927.5**	929.5
15-1	62.37	29.70	6.93	1.0	72.56	11.36	15.08	1.0	922.0**	924.0
15-2	61.74	29.40	6.86	2.0	71.82	11.25	14.93	2.0	917.0***	919.0
15-4	60.48	28.80	6.72	4.0	70.36	11.02	14.62	4.0	915.0***	917.0
15-6	59.22	28.20	6.58	6.0	68.89	10.79	14.32	6.0	975.0	977.0
17-0	72.25	15.0	12.75	-	77.39	5.75	16.53	0.33	895.0**	896.5
17-1	71.53	14.85	12.62	1.0	76.62	5.68	16.70	1.0	890.0**	892.0
17-2	70.81	14.70	12.50	2.0	75.84	5.63	16.53	2.0	884.0***	886.0
17-4	69.36	14.40	12.24	4.0	74.30	5.51	16.19	4.0	921.5***	923.5
17-6	67.92	14.10	11.99	6.0	72.74	5.40	15.86	6.0	980.0	982.0
19-0	63.75	25.0	11.25	-	72.32	9.57	17.75	0.36	874.0**	875.0
19-1	63.11	24.75	11.14	1.0	71.60	9.47	17.93	1.0	867.5**	870.0
19-2	62.475	24.50	11.025	2.0	70.88	9.37	17.75	2.0	861.5***	863.5
19-4	61.20	24.0	10.8	4.0	69.43	9.18	17.39	4.0	912.0***	914.0
19-6	59.925	23.5	10.575	6.0	67.99	8.99	17.02	6.0	972.5	974.5

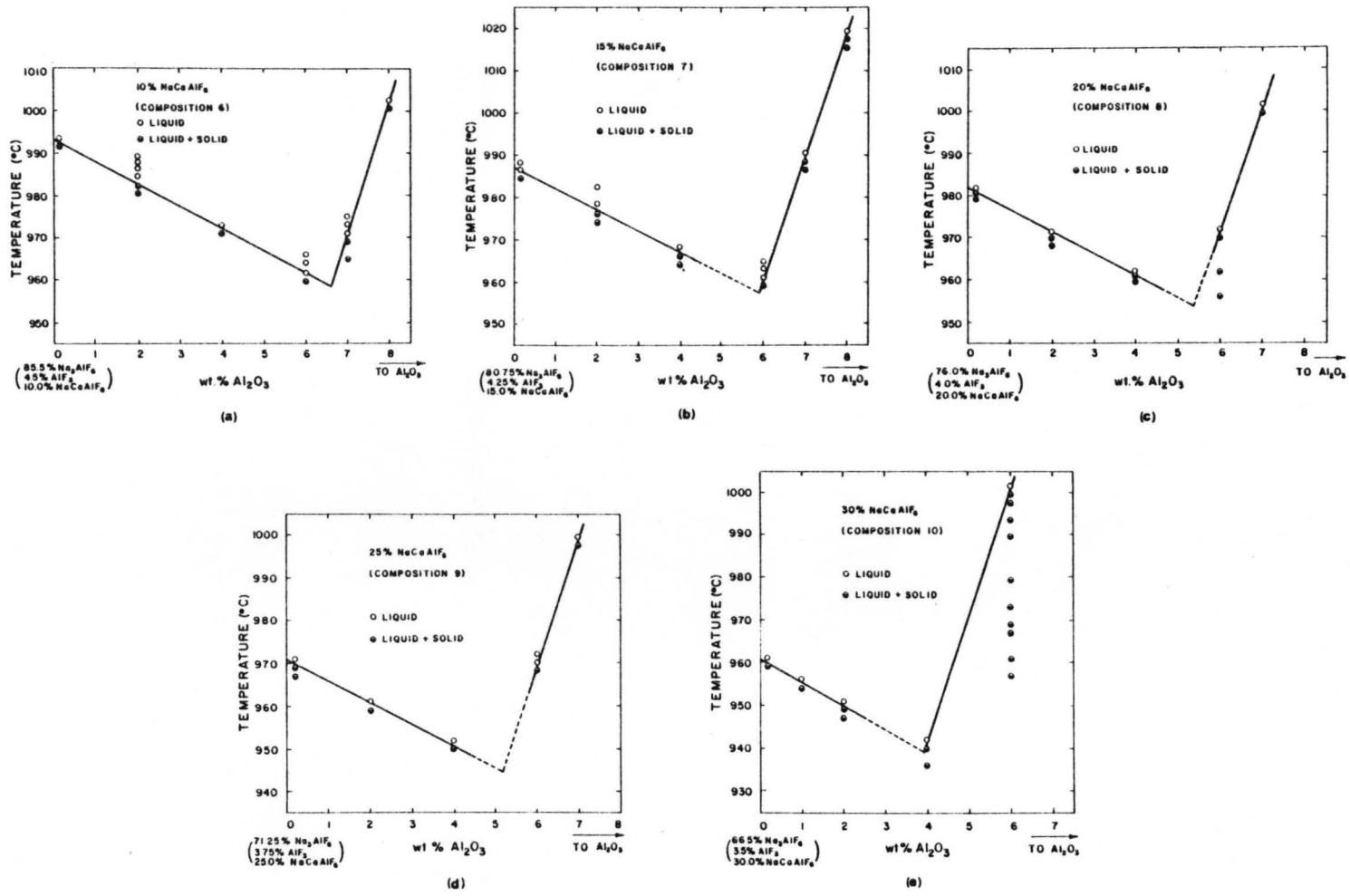

Fig. 18. The effect of Al_2O_3 on the liquidus temperatures of the join 95 Na_3AlF_6/5 AlF_3-$NaCaAlF_6$.

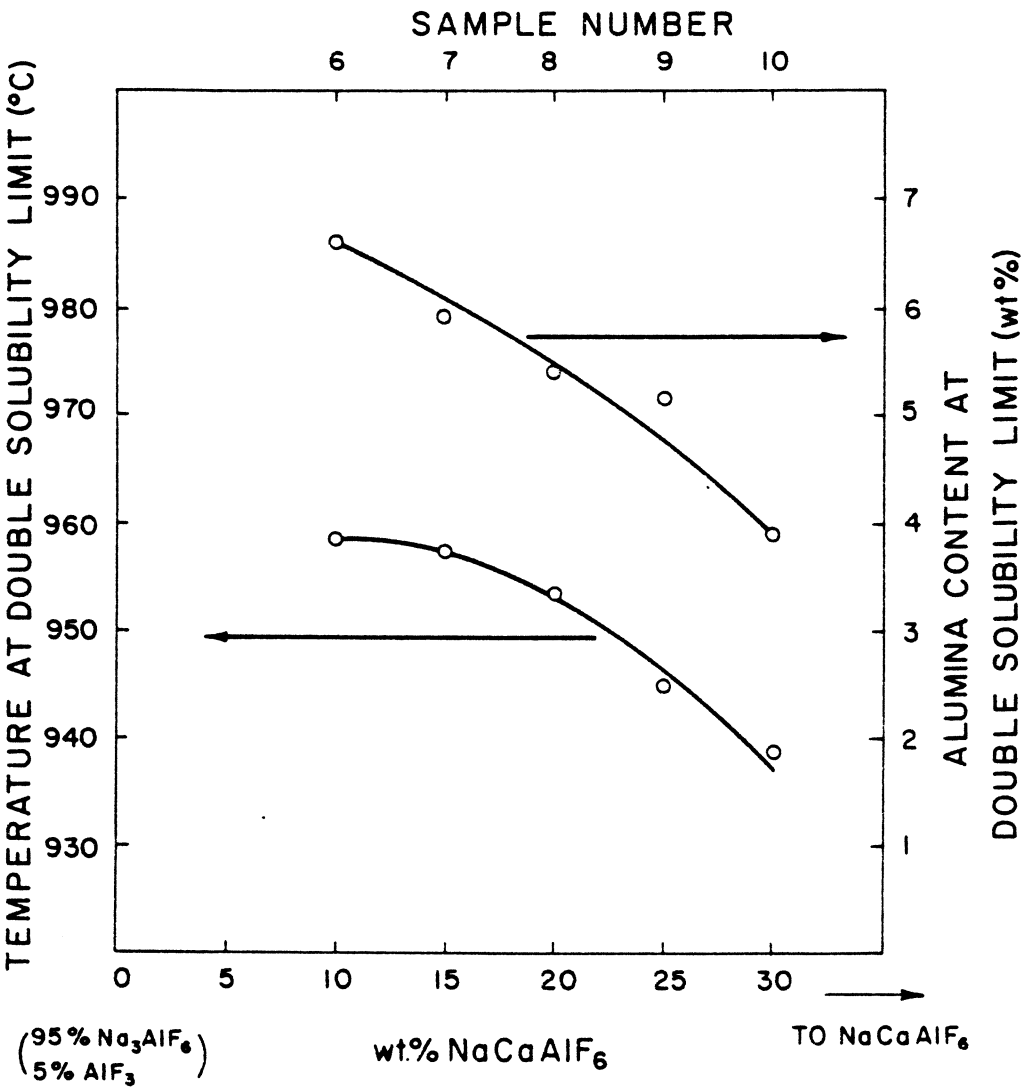

Fig. 18(f). The effect of Al_2O_3 on the temperatures and alumina contents at the double solubility limit of the join 95 Na_3AlF_6/5 AlF_3-$NaCaAlF_6$.

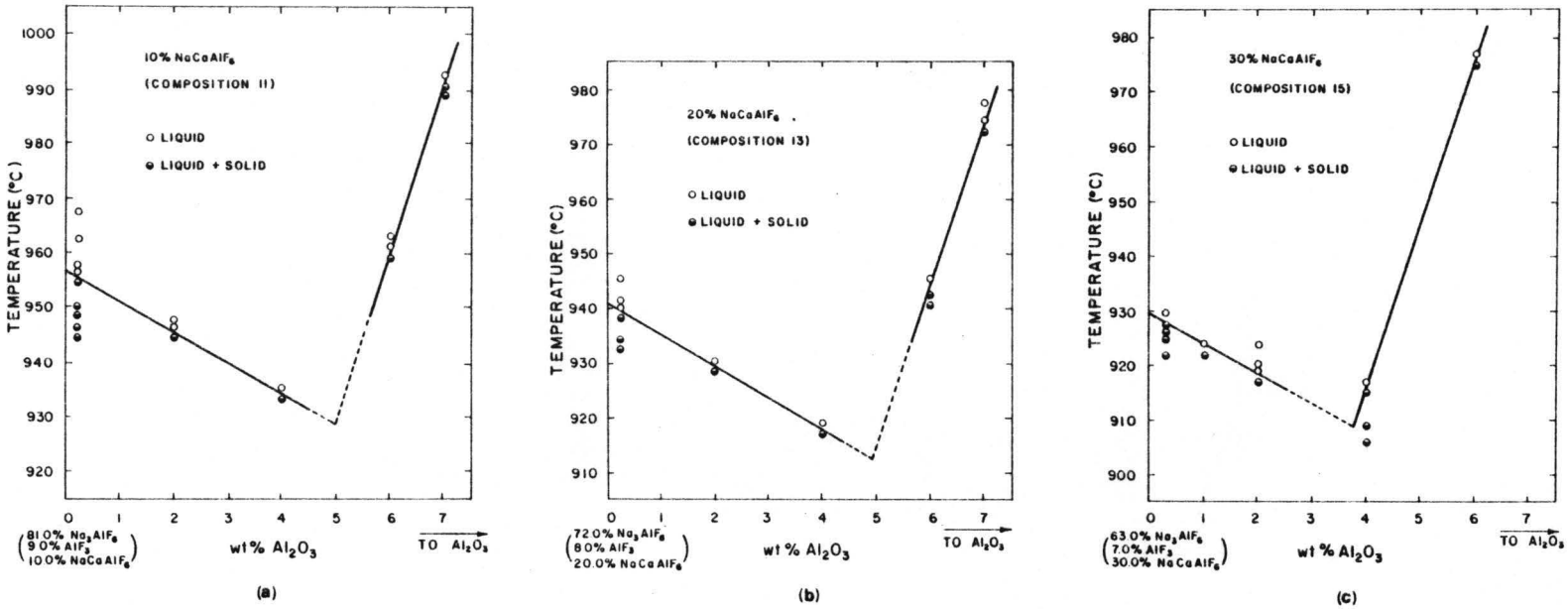

Fig. 19. The effect of Al_2O_3 on the liquidus temperatures of the join 90 Na_3AlF_6/10 AlF_3-$NaCaAlF_6$.

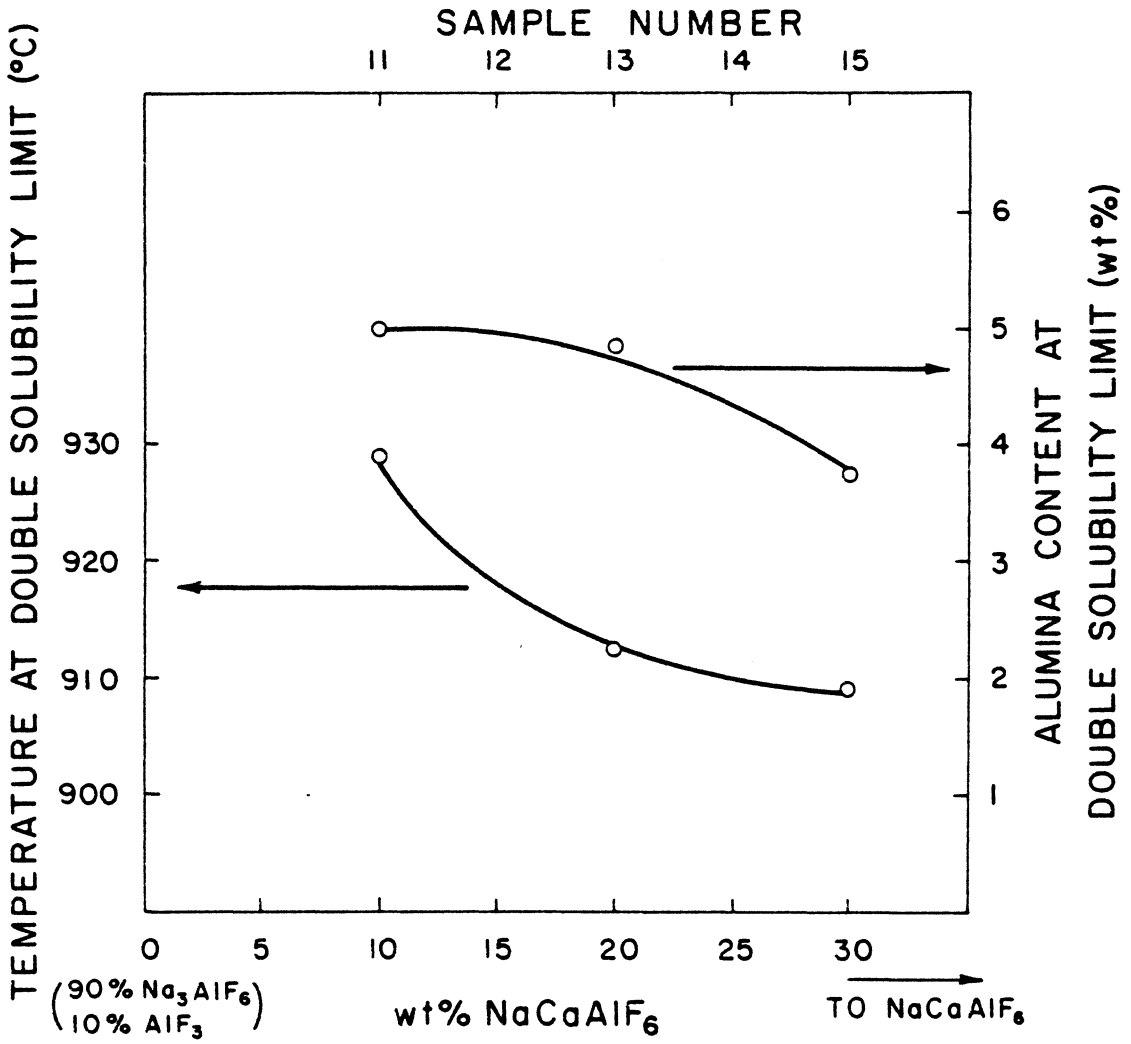

(d)

Fig. 19(d). The effect of Al_2O_3 on the temperatures and alumina contents at the double solubility limit of the join 90 Na_3AlF_6/10 AlF_3-$NaCaAlF_6$.

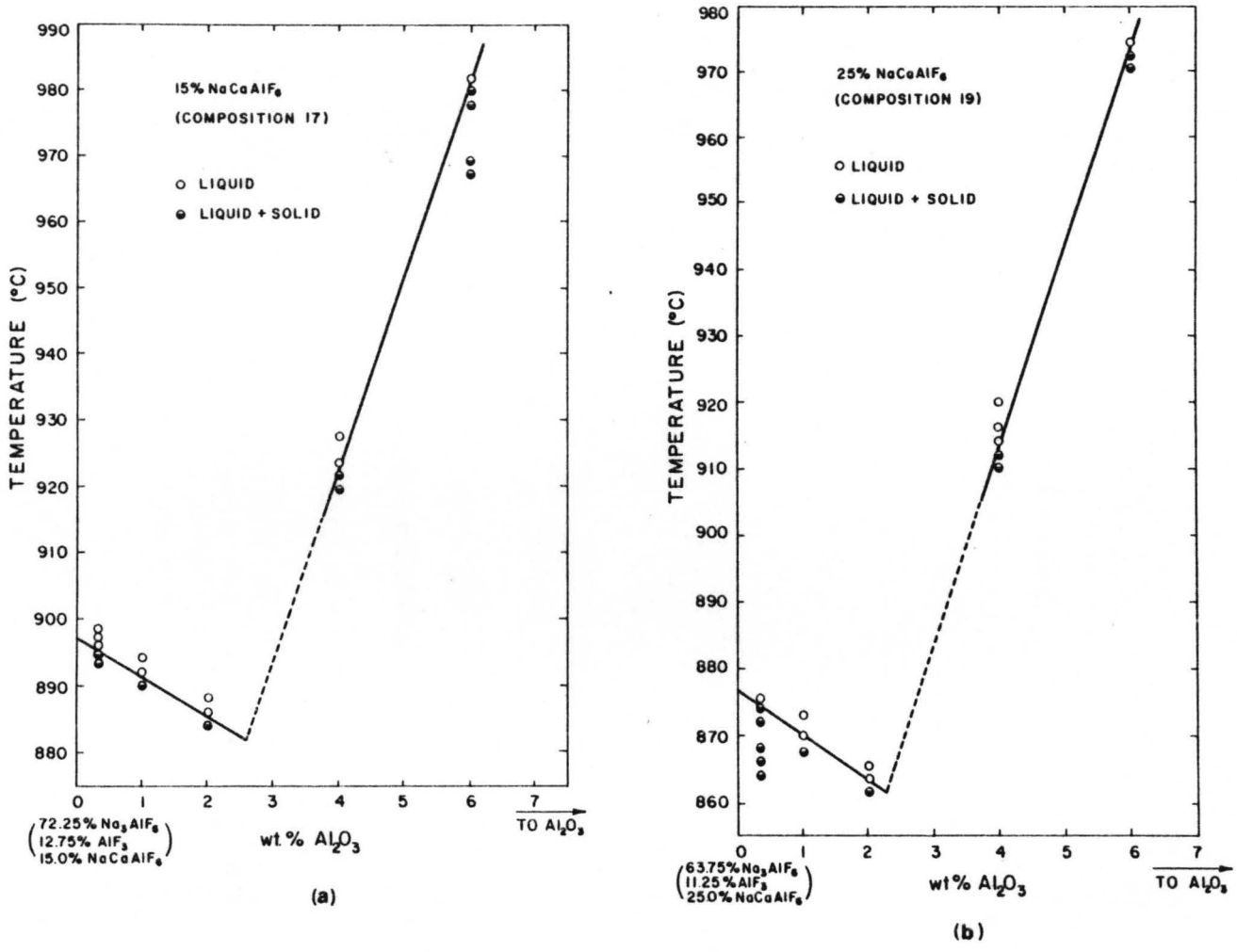

Fig. 20. The effect of Al_2O_3 on the liquidus temperatures of the join 85 Na_3AlF_6/15 AlF_3-$NaCaAlF_6$.

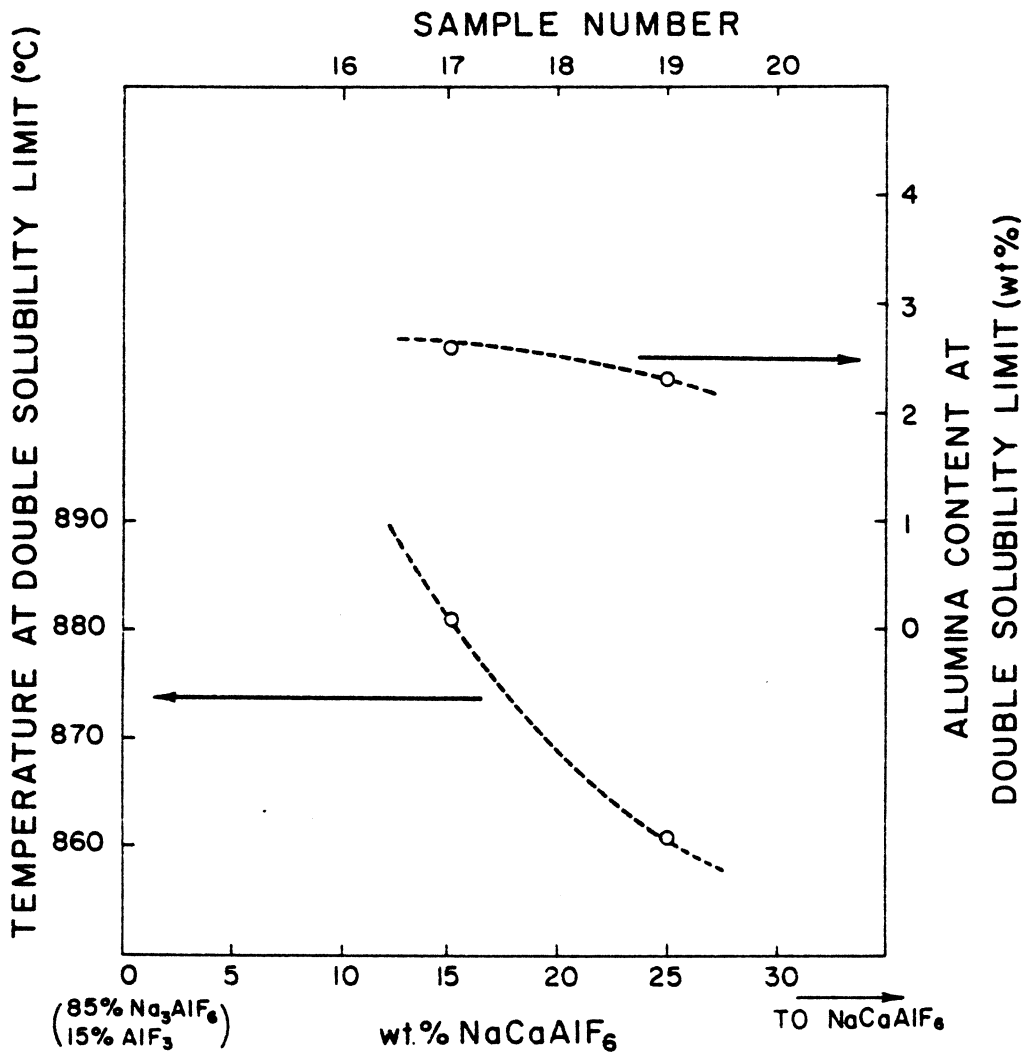

(c)

Fig. 20(c). The effect of Al_2O_3 on the temperatures and alumina contents at the double solubility limit of the join 85 Na_3AlF_6/15 AlF_3-$NaCaAlF_6$.

b) The cryolite liquidus temperature decreases with increasing Al_2O_3 content until the eutectic point is reached; thereafter, the corundum liquidus temperature increases with increasing alumina content.

c) For each pseudo-binary phase diagram, the temperature coefficients (i.e. the change of liquidus temperature with increasing 1 wt.% solute in a solution) for the cryolite liquidus and the corundum liquidus are listed in Table 4. The average temperature coefficients which are calculated by using sample mean and standard deviation of the mean are -5.33°C/wt.% Al_2O_3 and 30°C/wt.% Al_2O_3 for cryolite liquidus and corundum liquidus, respectively. These data agree with both Richard datum (~5.4°C/wt.% Al_2O_3 for cryolite) [24] and Brown and Lee's datum (~29°C/wt.% Al_2O_3 for corundum liquidus) [21].

d) For each join (e.g. compositions 6, 7, 8, 9, and 10), the temperatures and Al_2O_3 contents at the double solubility limit decrease with increasing $NaCaAlF_6$ content (Fig. 18 (f), Fig. 19 (d) and Fig. 20 (c)).

e) For the composition range now used in the Hall cell (80-86 wt.% Na_3AlF_6, 4-6 wt.% CaF_2, 5-10 wt.% AlF_3 and 3-5 wt.% Al_2O_3), which corresponds to compositions 6, 7, and 8, the alumina contents at the double solubility limit are, respectively, 6.6, 5.9 and 5.4 wt.% and the corresponding eutectic temperatures are respectively, 958.5°C, 957.5°C and 953.5°C. This means the operating temperature for

TABLE 4. STATISTICAL DETERMINATION OF TEMPERATURE COEFFICIENT OF Al_2O_3

Composition	Temperature Coefficients (°C/Wt.% Al_2O_3)	
	Cryolite Liquidus	Corundum Liquidus
6	-5.3	31.5
7	-5.0	29.25
8	-5.2	29.5
9	-5.1	29.5
10	-5.0	29.75
11	-5.5	31.5
13	-5.2	29.0
15	-5.5	33.0
17	-5.5	29.25
19	-6.0	30.1
Sample Mean (C/wt.% Al_2O_3)	-5.33	30.0
Standard Deviation of the Mean (°C/Wt.% Al_2O_3)	0.306	0.96

the cell may be as low as 975∿980°C (20°C above the eutectic temperature). For some compositions (e.g. compositions 11, 12, 13, 15, 16, 17, etc.) having a lower cryolite ratio than that of the Hall cell, the eutectic temperatures are lower. As a result, a lower operating temperature could conceivably be used. However, the alumina contents of the double solubility limit are less than 5 wt.%, some are even less than 3 wt.%. This is too low to make the cell composition hypoeutectic and near eutectic.

3) The Determination of Liquidus Temperature - Composition Relationship

In the quaternary system Na_3AlF_6-CaF_2-AlF_3-Al_2O_3, the temperature coefficient of Al_2O_3 is a constant, e.g. for cryolite liquidus, it is -5.33°C/wt.% Al_2O_3 no matter how the cryolite ratio is and how much the CaF_2 content is (Fig. 18, 19 and 20). However, the effects of CaF_2 and AlF_3 on the liquidus temperatures of cryolite-rich portion is not as simple as Al_2O_3.

In order to study the effects of CaF_2 and AlF_3 on the cryolite liquidus temperatures, an expression of liquidus temperature as a function of CaF_2, AlF_3 and Al_2O_3 contents was developed. Polynomial regression was used to fit the data listed in Table 2 and Table 3. The cryolite liquidus temperature may be expressed as:

$$T_{Liq.}(°C) = 1009.4+4.059(CaF_2) - 1.167(CaF_2)^2 + 0.968(CaF_2(AlF_3) - 0.105(CaF_2(AlF_3)^2 + 0.073(CaF_2)^2(AlF_3) + 0.002(CaF_2)^2 x (AlF_3) - 4.165(AlF_3) - 0.054(AlF_3)^2 - 5.33(Al_2O_3) \quad (9)$$

for CaF_2 3.8∿11.25%, AlF_2 5∿20%, where AlF_3, CaF_2 and Al_2O_3 are the weight percentages of AlF_3, CaF_2 and Al_2O_3 in the cryolite solution, respectively.

From this expression, it is obvious that the effects of CaF_2 and AlF_3 on the cryolite liquidus temperature are not independent. This is in agreement with thermodynamics principles. According to thermodynamics, if there are two or more solutes in a solution, the activity coefficient of any solution will be affected by the presence of the other solutes. The activity coefficient may be increased or decreased depending on the mutual action of the two solutes. Therefore, the effect of any component on the liquidus temperature will be affected by the presence of other components.

4) X-ray powder diffraction experiments were done for some samples (compositions 12, 15, 17, 19 and 85% Na_3AlF_6/15% AlF_3) which were quenched from the temperatures listed in Table 5.

TABLE 5. THE RESULTS OF X-RAY POWDER DIFFRACTION

Composition	Quenching Temperature (°C)	Liquidus Temperature (°C)	Crystal Existing in Diffraction Pattern
12	940	947.5	Na_3AlF_6+$Na_5Al_3F_{14}$
15	921	929	"
17	889	897	"
19	869	871	"
85% Na_3AlF_6/ 15% AlF_3	1000	960[27]	"

Diffraction patterns show that:

a) Compositions 12, 15, 17 and 19 quenched from the temperature a little lower than the liquidus temperature have cryolite diffraction lines. This results in agreement with optical microscopy examination (i.e. cryolite is a primary phase).

b) Sample containing 85% Na_3AlF_6/15% AlF_3 quenched from 1000°C which is much higher than the liquidus temperature shown in Foster's Na_3AlF_6-AlF_3 binary phase diagram (Fig. 16) also has cryolite diffraction lines.

c) All of these diffraction patterns have chiolite ($Na_5Al_3F_{14}$) diffraction lines.

Foster [27] studied the x-ray powder diffraction pattern of a sample with 57.5% Na_3AlF_6-42.5% AlF_3 quenched from liquid region. These results showed the presence of the diffraction lines of $Na_5Al_3F_{14}$ and $NaAlF_4$. He attributed the presence of these diffraction lines as due to short range order of $Na_5AlF_3F_{14}$ and $NaAlF_4$ in liquid phase.

In this study, microstructural examinations of all these five compositions showed that:

a) Some glassy phase contained bright crystals which has the same features as pure chiolite, e.g. the feature of cleavage (cf Fig. 21 and Fig. 10). This means that the occurrence of the diffraction lines of $Na_5Al_3F_{14}$ is due to the existence of chiolite in glassy phase.

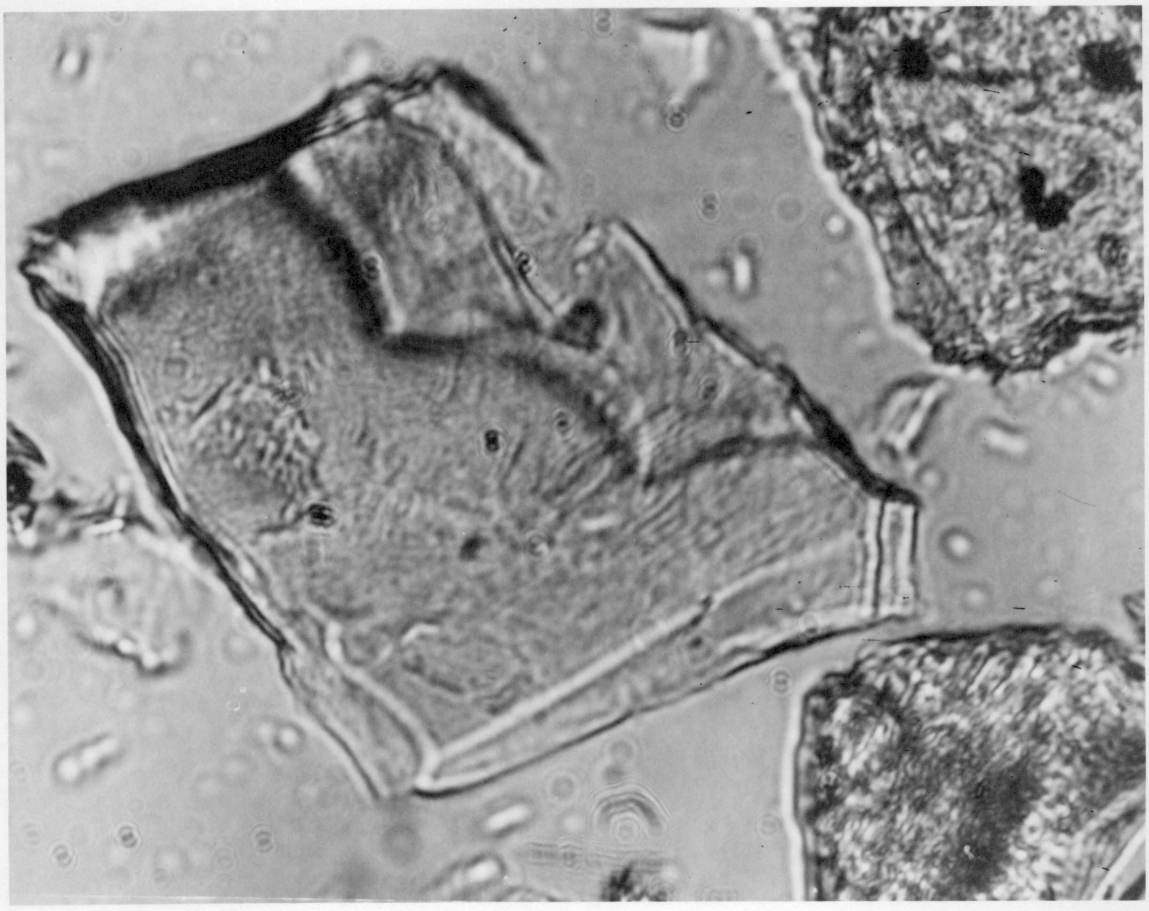

Fig. 21. Optical micrograph of quenched sample.
Sample: 77.40% Na_3AlF_6 5.74% CaF_2 16.53% AlF_3
0.33% Al_2O_3 quenched from 885°C

Refractive index of oil	1.3919
Microstructure	Glassy phase containing chiolite crystal
Magnification	584x

b) Other glassy phase contained tiny bright spots (Fig. 11 and Fig. 12) which were also shown under cross polarizer. If the x-ray diffraction lines of $Na_5Al_3F_{14}$ and Na_3AlF_6 for 85% Na_3AlF_6-15% AlF_3 quenched from 1000°C (liquid region) is considered, then these tiny bright spots in glassy phase may be postulated as Na_3AlF_6 crystals. Likewise, the tiny bright spots in glassy phase for compositions 12, 15, 17 and 19 may be Na_3AlF_6 crystals. This means for these four compositions, part of Na_3AlF_6 is in primary phase and part of Na_3AlF_6 in glassy phase.

This phenomena might be explained as the result of the intrinsic nature of the cryolite solution. Compared to silica, cryolite is a difficult glass-forming material, because (1) from thermodynamics calculation (appendix 1), the driving force ΔG for the crystallization of supercooled cryolite liquid is much higher than that of supercooled silica liquid, which is a typical glass-forming material; (2) the viscosity of cryolite solution is much lower than that of silica liquid, which would tend to increase the likelihood of crystallization; (3) Na_3AlF_6 is a more densely packed structure than SiO_2, so that it is difficult to form a random-network structure. Therefore, when cryolite liquid is quenched into cold water from high temperature, some tiny crystals (cryolite and/or chiolite) form before the formation of the glassy phase.

IV. CONCLUSION

1) The isotherms of the cryolite-rich portion of ternary system Na_3AlF_6-CaF_2-AlF_3 were obtained (Fig. 15).

2) The effects of Al_2O_3 on the cryolite liquidus and corundum liquidus have been studied. The temperature coefficients of Al_2O_3 for cryolite liquidus and corundum liquidus are -5.33°C/wt.% Al_2O_3 and 30°C/wt.% Al_2O_3, respectively.

3) Temperatures and the alumina contents at double solubility limit of 95% Na_3AlF_6/5% AlF_3-Al_2O_3, 90% Na_3AlF_6/10% AlF_3-Al_2O_3 and 85% Na_3AlF_6/15% AlF_3-Al_2O_3 joins have been obtained (Fig. 18, 19 and 20). For the compositions of these joins, the alumina contents at double solubility limit is 2.5∿6 wt.% Al_2O_3.

4) For the composition range used in the Hall cell, the alumina content and temperature at double solubility limit are 5.4-6.6% Al_2O_3 and 953.5∿958.5°C, that means the operating temperature is 975∿980°C.

5) The liquidus temperature of the quaternary system Na_3AlF_6-CaF_2-AlF_3-Al_2O_3 for CaF_2 3.8∿11.25%, AlF_3 5∿20% might be expressed as:

$$\begin{aligned} T_{Liq.}(°C) = {} & 1009.4 + 4.059(CaF_2) - 1.167(CaF_2)^2 + \\ & 0.968(CaF_2)(AlF_3) - 0.105(CaF_2)(AlF_3)^2 + \\ & 0.073(CaF_2)^2(AlF_3) + 0.002(CaF_2)^2(AlF_3)^2 \\ & - 4.165(AlF_3) - 0.054(AlF_3)^2 - 5.33(Al_2O_3) \end{aligned}$$

6) Cryolite and chiolite crystals existing in glassy phase have been observed. The existence might be due to the difficulty of forming a fluoride glass.

REFERENCES

[1] K. Grjotheim et al., Aluminium Electrolysis, Chapter 1.

[2] J. B. Todd, Light Metals, 1981, p. 1023-1036.

[3] G. T. Holmes, Light Metals, 1980, p. 401.

[4] R. T. Poole and C. Etheridge, Light Metals, 1977, v. 1, p. 163-183.

[5] J. Thoustad and Ye-Xiang Liu, Light Metals, 1981, p. 303-312.

[6] D. Bratland, K. Grjotheim and C. Krohn, Light Metals 1976, p. 3-21.

[7] P. Aeschbach and H. Friedli, Light Metals, 1981, p. 389-396.

[8] Yamada, Koichi, et al., U.S. Patent 4,039,401, 1977.

[9] K. Matiasovsky, Electrochem. Soc., v. 111, 1960, p. 973-976.

[10] P. A. Foster, Jr., J. Am. Cer. Soc., v. 43, 1960, p. 66-68.

[11] E. W. Dewing, Canadian Metall. Quart., v. 3, 1974, p. 607-618.

[12] E. W. Dewing and P. Desclaux, Trans. Met., 8B, 1977, p. 555-561.

[13] K. Matiasovsky et al., Electrochem. Soc., v. 116, 1969, p. 1381-1383.

[14] D. F. Craig, Dissertation, Virginia Polytechnic Institute and State University, Blacksburg, VA, 1977.

[15] M. Rolin, Bull. Soc. Chim, 1961, p. 1120-1125.

[16] P. A. Foster, Jr., J. Am. Cer. Soc., v. 58, 1975, p. 288-291.

[17] G. A. Abramov et al., Elektromet. Tsvetnykh Metal., 1957, No. 188, p. 45-57.

[18] P. A. Foster, Jr., J. Am. Cer. Soc., v. 43, 1960, p. 437-438.

[19] A. Fennerty and E. A. Hollingshead, J. Electrochem. Soc., v. 107, 1960, p. 993-997.

[20] M. Rolin, Bull. Soc. Chem., 1961, p. 1404-1407.

[21] S. Lee, Thesis, Virginia Polytechnic Institute and State University, 1981.

[22] K. S. Lei, Thesis, Virginia Polytechnic Institute and State University, 1981.

[23] E. W. Dewing, J. Electrochem. Soc., v. 117, 1970, p. 780-781.

[24] M. C. Richard, Light Metals, 1975, p. 95-103.

[25] F. D. Bloss, An Introduction to the Methods of Optical Crystallography, Chapter 5, 1961, Holt Rinehart and Winston Inc.

[26] W. L. Roberts, G. R. Papp, Jr. and J. Weber, Encyclopedia of Minerals, 1974, Van Nostrard Peinhold.

[27] P. A. Foster, Jr., J. Am. Cer. Soc., v. 53, 1970, p. 598-600.

[28] J. L. Holm, Acta Chem. Scand., v. 22, 1968, p. 1004-1012.

[29] U.S. Bureau of Mines Bulletin, 584, p. 94, 160, 176.

APPENDIX 1

Comparison of driving force ΔG for crystallization between Na_3AlF_6 and SiO_2.

As mentioned above, cryolite is not a glass-forming material. In order to describe the difficulty of glass formation for cryolite system, the calculation of driving force ΔG for crystallization under supercooling is necessary. It is known that the greater the driving force for crystallization, the smaller the tendency to the formation of glassy phase during quenching.

The difference of free energy between supercooling liquid and crystal ΔG, which is a function of temperature, can be calculated by using Gibbs-Helmholtz equation

$$\left[\frac{d\left(\frac{\Delta G}{T}\right)}{d\left(\frac{1}{T}\right)}\right]_p = \Delta H \qquad \text{(A-1)}$$

where ΔH, the difference of heat contents between supercooling liquid and crystal, is a function of temperature T and can be calculated by integrating:

$$d(\Delta H) = \Delta C_p dT \qquad \text{(A-2)}$$

where $$\Delta C_p = C_p(\text{crystal}) - C_p(\ell)$$

$$= \Delta a + \Delta bT + \Delta CT^{-2} \qquad \text{(A-3)}$$

if it is assumed that $C_p = a + bT + CT^{-2}$. The constant a, b and c for liquid and crystal can be found in the literature [29].

Therefore, ΔH and ΔG can be expressed as follows by integrating (A-1) and (A-2).

$$\Delta H = \Delta H_o + \Delta aT + \frac{\Delta b}{2} T^2 - \frac{\Delta C}{T} \qquad \text{(A-4)}$$

$$\Delta G = \Delta H_o - \Delta a\, T \ln T - \frac{\Delta b}{2} T^2 - \frac{\Delta C}{T} + IT \qquad \text{(A-5)}$$

where ΔH_o and I are the constants of integration and can be obtained by using certain boundary conditions, such as

$$\text{at } T = T_{equi.} \qquad \Delta H = \Delta H_{freezing}, \quad \Delta G = 0$$

The purpose of this calculation is to explain the diffuculty of glass formation for cryolite system by comparing $\Delta G(= G_{crys.} - G_{\ell})$ at supercooling condition of SiO_2 (glass-easy formation system) and Na_3AlF_6. Table A-1 shows the result of the calculations.

Obviously, the difference of Gibbs free energy between undercooling liquid and crystal ΔG for cryolite is much higher than that for SiO_2. Therefore, this is one reason for the difficulty of forming a cryolite glassy phase when liquid is quenched into cold water.

TABLE A-1. COMPARISON OF THE DRIVING FORCE ΔG FOR CRYSTALLIZATION OF DIFFERENT SYSTEMS

	SiO_2	$Fe_{0.947}O$	Na_3AlF_6
Heat Capacity of Crystal $C_{p(c)}$ (cal/mole°K	$14.40+2.04\times10^{-3}T$ (Cristobalite) (523° - 2000°K)	$11.66+2.0\times10^{-3}T$ $-0.67\times10^{5}T^{-2}$ (298° - 1650°K)	$52.15+15.86\times10^{-3}T$ (845° - 1300°K)
Heat Capacity of Liquid $C_{p(\ell)}$(cal/mole°K)	$13.38+3.68\times10^{-3}T$ $-3.45\times10^{5}T^{-2}$ (298° - 2000°K)	16.30 (1650° - 2000°K)	93.40 (1300° - 1500°K)
Freezing Point (°K)	1996	1650	1300
ΔH(freezing) (cal/mole)	-789.92	-7490	-27,640
ΔH (T) (cal/mole)	$596+1.02T-0.82\times10^{-3}T^2-\frac{3.45\times10^5}{T}$	$-2597.11-4.64T+1.0\times10^{-3}T^2+\frac{0.67\times10^5}{T}$	$12583.3-41.25T+7.93\times10^{-3}T^2$
ΔG (T) (cal/mole)	$596-1.02T\ell nT+0.82\times10^{-3}T^2-\frac{3.45\times10^5}{2T}+5.859T$	$-2597.11+4.64T\ell nT-1.0\times10^{-3}T^2+\frac{0.67\times10^5}{2T}-31.164T$	$12583.3+41.25T\ell nT-7.93\times10^{-3}T^2-295.14T$
ΔG at different supercooling (cal/mole)			
100°K	-35.1	-449.7	-2045.1
200°K	-59.44	-889.05	-3901.9
300°K	-73.92	-1316.16	-5541.79

The vita has been removed from the scanned document